

Brain Insulin-Like Growth Factor-I Directs the Transition from Stem Cells to Mature Neurons During Postnatal/Adult Hippocampal Neurogenesis

VANESA NIETO-ESTÉVEZ,^{a,b} CARLOS O. OUESLATI-MORALES,^{a,b} LINGLING LI,^a JAMES PICKEL,^c AIXA V. MORALES,^a CARLOS VICARIO-ABEJÓN^{a,b}

Key Words. Brain IGF-I • Neural stem cells • Neurogenesis • Hippocampus • Conditional knockout

^aInstituto Cajal, Consejo Superior de Investigaciones Científicas (CSIC), ^bCentro de Investigación Biomédica en Red sobre Enfermedades Neurodegenerativas (CIBERNED), Madrid, Spain; ^cTransgenic Core, National Institute of Mental Health, National Institutes of Health, Bethesda, Maryland, USA

Correspondence: Dr. Carlos Vicario-Abejón, Instituto Cajal, CSIC, Avenida Doctor Arce 37, E-28002 Madrid, Spain. Telephone: (+34) 91-585-4721; Fax: (+34) 91-585-4754; e-mail: cvicario@cajal.csic.es

Received July 17, 2015; accepted for publication April 11, 2016; first published online in STEM CELLS EXPRESS May 04, 2016.

© AlphaMed Press
1066-5099/2016/\$30.00/0

<http://dx.doi.org/10.1002/stem.2397>

ABSTRACT

The specific actions of insulin-like growth factor-I (IGF-I) and the role of brain-derived IGF-I during hippocampal neurogenesis have not been fully defined. To address the influence of IGF-I on the stages of hippocampal neurogenesis, we studied a postnatal/adult global *Igf-1* knockout (KO) mice (*Igf-1*^{-/-}) and a nervous system *Igf-1* conditional KO (*Igf-1*^{Δ/Δ}). In both KO mice we found an accumulation of Tbr2⁺-intermediate neuronal progenitors, some of which were displaced in the outer granule cell layer (GCL) and the molecular layer (ML) of the dentate gyrus (DG). Similarly, more ectopic Ki67⁺-cycling cells were detected. Thus, the GCL was disorganized with significant numbers of Prox1⁺-granule neurons outside this layer and altered morphology of radial glial cells (RGCs). Dividing progenitors were also generated in greater numbers in clonal hippocampal stem cell (HPSC) cultures from the KO mice. Indeed, higher levels of *Hes5* and *Ngn2*, transcription factors that maintain the stem and progenitor cell state, were expressed in both HPSCs and the GCL-ML from the *Igf-1*^{Δ/Δ} mice. To determine the impact of *Igf-1* deletion on neuronal generation in vivo, progenitors in *Igf-1*^{-/-} and *Igf-1*^{+/+} mice were labeled with a GFP-expressing vector. This revealed that in the *Igf-1*^{-/-} mice more GFP⁺-immature neurons were formed and they had less complex dendritic trees. These findings indicate that local IGF-I plays critical roles during postnatal/adult hippocampal neurogenesis, regulating the transition from HPSCs and progenitors to mature granule neurons in a cell stage-dependent manner. STEM CELLS 2016; 00:000–000

SIGNIFICANCE STATEMENT

There is evidence that systemic insulin-like growth factor-I (IGF-I) promotes neuronal maintenance in the postnatal/adult hippocampus. Other studies have suggested the implication of locally-produced IGF-I in the modulation of adult hippocampal neurogenesis in vivo but this concept was not demonstrated. We present novel findings showing that brain IGF-I directs the generation of granule neurons from neural stem cells in the postnatal/adult mouse hippocampus. We also show that the regulation of gene expression and cycling cell number by IGF-I may be part of the mechanisms involved in these actions.

INTRODUCTION

The formation of new neurons persists in the postnatal and adult mammalian hippocampus (HP) due to the existence of neural stem cells (NSCs) located in the subgranular zone (SGZ) of the DG [1–3]. These NSCs (or type I cells) are quiescent cells, yet upon activation they self-renew to maintain the NSC population and to produce dividing neuronal progenitors that will differentiate into granule neurons [4–7]. Significantly, the maintenance and proliferation of adult NSCs, and the generation, migration and differentiation of newly formed neurons, are regulated by extracellular growth factor signaling [8, 9].

While circulating IGF-I promotes neuronal survival and adult neurogenesis, its specific effects and mechanisms of action are still not fully understood. Similarly, the role of locally-produced IGF-I in regulating adult neurogenesis remains to be determined [10–16]. Conditional deletion of the *Igf-1* receptor gene (*Igf-1R*) using the Nestin-Cre strategy produces almost complete loss of the DG in mice [17]. Moreover, exogenous IGF-I promotes the proliferation of progenitor cells in the adult HP, both in culture and in vivo [18–22]. This enhancement in cell proliferation is followed by the formation of granule neurons [18, 20, 23]. By contrast, there are more proliferative

cells in the SGZ of adult *Igf-1* KO mice [24], although both the *Igf-1* KO and the *Igf-1R* KO have fewer granule and parvalbumin (PV)⁺ neurons [24–26] indicating that the influence of IGF-I on proliferation and differentiation remains unclear.

Furthermore, our studies demonstrated that IGF-I plays a critical role in regulating the exit of neuroblasts from the subventricular zone (SVZ) and the incorporation of new neurons into the adult olfactory bulb (OB), in part through the activation of the PI3K/AKT pathway [12]. However, IGF-I effects on hippocampal cell migration/positioning were not reported [12, 27–30].

In previous studies, a role for local IGF-I on regulating adult neurogenesis was suggested but no *in vivo* work has demonstrated this concept [12, 14, 24, 31–34]. Thus, we have analyzed the influence of the lack of IGF-I on the different stages of neurogenesis in the postnatal/adult DG. Furthermore, we have generated a nervous system specific *Igf-1* conditional KO mouse to study the role of brain IGF-I on neurogenesis. Taken together, our results indicate that local IGF-I directs the transition from HPSCs and progenitors to granule neurons. Moreover, this factor promotes the correct migration/positioning as well as the morphological and molecular maturation of these neurons. Our findings suggest that these effects might be dependent on the regulation of *Hes5* and *Ng2* expression and cycling cell number by IGF-I.

MATERIALS AND METHODS

Global *Igf-1* Knockout Mice (*Igf-1*^{-/-})

We used mice obtained from the mating of MF1 *Igf-1*^{+/-} mice [12, 35–37].

Conditional *Igf-1* Knockout Mice, Nestin-Cre:*Igf-1* (*Igf-1*^{Δ/Δ})

To study the role of IGF-I produced locally in the brain and to prevent the death of the global *Igf-1* KO mice caused by the lack of lung maturation [36], we have generated a conditional *Igf-1* KO mice in which *Igf-1* is deleted specifically in neural cells by crossing an *Igf-1* loxP line mice [38] with a Nestin-Cre line mice [39–41] purchased from The Jackson Laboratory (Bar Harbor, Maine, USA <https://www.jax.org/>).

To verify that the production of Cre was specific to the neural cells, we crossed Nestin-Cre mice with the Rosa26-Yellow fluorescent protein (YFP) reporter mice [42].

The conditional *Igf-1* KO mice were maintained by crossing C57Bl6N *Igf-1*^{Δ/Δ} mice. In this work we have analysed 19 conditional *Igf-1* KO mice (*Igf-1*^{Δ/Δ}) and 20 control mice (7 *Igf-1*^{+/+}, 4 *Igf-1*^{fl/fl}, 1 *Igf-1*^{+/fl} and 8 *Igf-1*^{+/+} Cre⁺ mice). We did not find statistically significant differences between the mice used as controls (hereafter referred to as *Igf-1*^{Ctrl}) and accordingly the results obtained were combined in the study. The genotypes of the different mice were determined by PCR on tail DNA (Supporting Information Tables S1, S2).

All animal care and handling was carried out in accordance with European Union guidelines and Spanish legislation.

In vivo Injection of Retroviral Vectors Expressing Enhancer Green Fluorescent Protein (EGFP)

Retroviral particles expressing EGFP under the control of a CMV promoter were obtained by transfecting the retroviral

plasmid into 1F8 cells [43, 44]. The titers of the concentrated viral particles were in the range of 10¹³ colony forming units (cfu)/ml. Particles (2 μl) were injected stereotaxically into the hilus (Hi) of the DG of anesthetized postnatal day 21 (P21) *Igf-1*^{+/+} and *Igf-1*^{-/-} mice and the animals were analyzed 21 days postinjection (dpi). The stereotaxic coordinates were: anteroposterior to bregma $-(d + 0.2)$ mm, lateral to midline 1.9 mm and ventral to dura -2 mm in *Igf-1*^{+/+} mice; and anteroposterior to bregma $-(d + 0.1)$ mm, lateral to midline 1.2 mm, ventral to dura -1.6 mm in the *Igf-1*^{-/-} mice, where “*d*” is half the length between bregma and lambda.

Immunohistochemistry

Cryostat (15 μm) and vibratome (50 μm) sections were incubated for 24–72 hours at 4°C with the primary antibodies listed in Supporting Information.

Quantitative Analysis of Immunostained Sections

The number of Nestin⁺, Sox2⁺, BrdU⁺, Ki67⁺, MCM2⁺, Pax6⁺, Tbr2⁺, Doublecortin (DCX)⁺, and Prox1⁺ cells was quantified in confocal images of single optical planes taken every 2 μm along the thickness (z-axis) of the sections.

To analyze the percentage of cells exiting the cell cycle *in vivo*, adult *Igf-1*^{Ctrl} and *Igf-1*^{Δ/Δ} mice were injected with a single dose of 5-bromo-2'-deoxyuridine (BrdU, 100 μg/g) 24 hours before perfusion. After immunostaining, the number of BrdU⁺ and Ki67⁺ cells were counted.

The process length of the Nestin⁺ cells was measured using ImageJ software (NIH, <https://imagej.nih.gov/ij/>) and the number of secondary processes or branches was counted in ten cells per animal.

The distribution of labeled cells in the different subdivisions of the DG [SGZ, inner granule cell layer (iGCL), outer granule cell layer (oGCL) and molecular layer (ML)] was analyzed and the results were expressed as the percentage of cells positive for each marker in each subdivision.

The main dendrite length of the DCX⁺ cells was measured using ImageJ software in ten cells per animal.

The number of ectopic Prox1⁺ granule neurons was counted in confocal images of single optical planes. To mark the granule cell layer (GCL), we measured the fluorescence intensity of Prox1⁺ cells from the Hi to the hippocampal fissure (HF) or ventricle (see plots in Fig. 3I). Accordingly, we drew a line across the GCL where the Prox1 intensity increases sharply between the Hi and the GCL, and it decreases sharply between the GCL and ML. We choose the immunostaining of Prox1 to delineate the GCL as this transcription factor specifically labels granule neurons [45, 46].

The percentage of cells expressing DCX, Calretinin (CR), Calbindin (CB) and Prox1 of the total GFP⁺-cells at 21 dpi was counted in confocal images of single optical planes taken every 2 μm through the thickness of the sections.

The total length of the GFP⁺-cells was determined using ImageJ, and the number of primary dendrites and branches were counted directly. We also analyzed the distribution of GFP⁺-cells in the SGZ, iGCL, oGCL and ML as described above.

In Situ Hybridization

In situ hybridization with a digoxigenin-labeled *Igf-1* probe was performed following standard methods in cryostat sections from P21 and P49 *Igf-1*^{+/+} and *Igf-1*^{-/-} mice.

Neural Stem Cell Cultures

HPSCs were prepared from single P21 *Igf-1^{+/+}* and *Igf-1^{-/-}* mice, from adult (6-month-old) *Igf-1^{Ctrl}* and *Igf-1^{Δ/Δ}* mice, and from P21 C57Bl6N mice essentially as described previously [47]. The resulting cells were cultured in Dulbecco's modified Eagle medium (DMEM)/nutrient mixture F12 (F12), supplemented with insulin (final concentration 10 μg/ml), apotransferrin, putrescine, progesterone, sodium selenite (N2; DMEM/F12/N2) and maintained with daily addition of 20 ng/ml fibroblast growth factor-2 (FGF-2, Peprotech Cat No. 100-18B, <https://www.peprotech.com/en-US>) and 20 ng/ml epidermal growth factor (EGF, Peprotech Cat No. AF-100-15). After cell passage 3 the insulin concentration was reduced to 0.5 μg/ml (87.2 nM) in cultures from *Igf-1^{+/+}*, *Igf-1^{-/-}*, *Igf-1^{Ctrl}* and *Igf-1^{Δ/Δ}* mice.

For the clonal analysis, neurospheres were dissociated and cells were seeded in 96-multiwell plates. The following day, wells containing a single cell were marked and then maintained 14 days when they were scored for the presence of single cells, duplets, groups of 4–8 cells, and neurospheres.

To analyse the percentage of cycling cells and cell cycle exit, adult HPSC (aHPSC) neurospheres from 6 month-old *Igf-1^{Ctrl}* and *Igf-1^{Δ/Δ}* mice were maintained as floating neurospheres adding FGF-2 and EGF every three days (partial deprivation), a condition that induces the initiation of differentiation in proliferating NSCs [48]. Neurospheres were given a pulse of BrdU 22 hours before splitting and the dissociated cells were cultured for 1 day in vitro (DIV) in the total absence of exogenous EGF and FGF-2 to induce differentiation.

To determine the expression of *Igf-1* and *Igf-1r* during aHPSC proliferation and differentiation, cells prepared from *Igf-1^{+/+}*, *Igf-1^{-/-}* and C57Bl6N mice were grown as neurospheres; then induced to differentiate upon growth factor removal for 1 and 2 days.

Fibroblast Cultures

Fibroblasts were isolated from small pieces of skin (~ 1 cm²) from the pectoral region of 2 to 20-month-old *Igf-1^{Ctrl}* and *Igf-1^{Δ/Δ}* mice. After 3–4 passages, cells were collected in TRIzol to extract RNA.

Hepatocyte Cultures

Hepatocytes were isolated from 2 to 20-month-old *Igf-1^{Ctrl}* and *Igf-1^{Δ/Δ}* mice. After 3–4 DIV, the cells were harvested in TRIzol to extract RNA.

Gene Expression Analysis in HPSCs

For gene expression analysis, HPSCs from *Igf-1^{Ctrl}* and *Igf-1^{Δ/Δ}* mice were seeded at 5,000 cells/cm² in DMEM/F12/N2 under FGF-2 and EGF partial deprivation. After six DIV the cells were recovered for RNA extraction followed by real-time reverse transcription quantitative-polymerase chain reaction (RT-qPCR) analysis using the primers listed in Supporting Information Table S3. Then, gene expression changes *Igf-1^{Δ/Δ}* mice were compared relative to the levels of gene expression obtained in *Igf-1^{Ctrl}* mice, using the CT method [49, 50] and were expressed as fold changes in log₂ scale. The expression of *Igf-1* in HPSCs, olfactory bulb stem cells (OBSCs), fibroblasts and hepatocytes obtained from *Igf-1^{Ctrl}* and *Igf-1^{Δ/Δ}* mice was also measured by (RT-qPCR) and the results were given as relative mRNA levels normalized to the Ct value for *Gapdh*. Similarly, the expression

of *Igf-1* and *Igf-1r* in HPSCs from *Igf-1^{+/+}*, *Igf-1^{-/-}* and C57Bl6N mice was also measured by RT-qPCR.

Gene Expression Analysis in Microdissected GCL-ML

Although the large majority of Ki67⁺, MCM2⁺, Pax6⁺, Tbr2⁺, and Prox1⁺ are located in the GCL a small yet significant proportion of them are found in the ML of *Igf-1* knockout mice (Figs. 1–6). Accordingly, the expression of *Igf-1*, *Hes5* and *Ngn2* was analyzed in the GCL-ML subregion, which was previously microdissected from 2-month old *Igf-1^{Ctrl}* and *Igf-1^{Δ/Δ}* mice.

IGF-I Immunoassay

The blood was extracted from the heart of 2 to 20-month-old *Igf-1^{Ctrl}* and *Igf-1^{Δ/Δ}* mice and was incubated at 37°C 1 hour and, then, at 4°C overnight. Serum IGF-I level was measured using a mouse IGF-I immunoassay following the manufacturer's instructions (Quantikine Enzyme-Linked Immunosorbent Assay, ELISA, mouse/rat IGF-I Immunoassay, R&D No. MG100, <https://www.rndsystems.com/>).

Statistical Analysis

A two-tailed Student's *t*-test was used to compare the mean ± SEM values from the *Igf-1^{+/+}* and *Igf-1^{-/-}* mice or *Igf-1^{Ctrl}* and *Igf-1^{Δ/Δ}* mice, with Welch's correction when the *F*-test indicated significant differences between the variances of both groups. To compare the raw mRNA values in linear scale obtained by RT-qPCR from *Igf-1^{Ctrl}* and *Igf-1^{Δ/Δ}* mice we used the nonparametric Wilcoxon test or the two-tailed Student's *t*-test. All analyses were carried out with GraphPad Prism software and the differences were considered as statistically significant when *p* < 0.05.

The full description of the Materials and Methods is given as Supporting Information.

RESULTS

The Cellular Expression of IGF-I and IGF-IR in the Postnatal/Adult HP

Although the regional expression of *Igf-1* and *Igf-1r* mRNAs in the central nervous system (CNS) is well characterized (Allen Brain Atlas and [11, 31, 34, 51–54]), their cellular distribution has been relatively less well studied [12, 34, 55–57]. Here, we analyzed the expression of IGF-I and IGF-IR protein and mRNA in different cell types of the postnatal/adult HP by single and dual immunohistochemistry, in situ hybridization and RT-qPCR (Supporting Information Figs. S1, S2).

We found IGF-I-immunoreactive cells in the Hi and the GCL of the DG, as well as in pyramidal cells of the CA3 region (Supporting Information Fig. S1A). Of these IGF-I⁺-cells, 42 % colocalized with PV (Supporting Information Fig. S1B–S1D) and an apparently smaller percentage (not quantified) colocalized with Prox1 (Supporting Information Fig. S1E–S1G). However, immunohistochemistry of HP sections from *Igf-1^{-/-}* mouse with our anti-IGF-I antibody (rabbit anti-IGF-I, IBT Ref. <http://www.ibtsystems.de/>: PABCa, <https://www.rndsystems.com/>) revealed positive staining (data not shown). The same result was obtained using two more antibodies: R&D Ref.: AF791 and Santa Cruz Ref.: sc-9013, <http://www.scbio.de/>. Thus, the specificity of the three antibodies could not be confirmed in the *Igf-1^{-/-}* mouse, a fact probably due to the

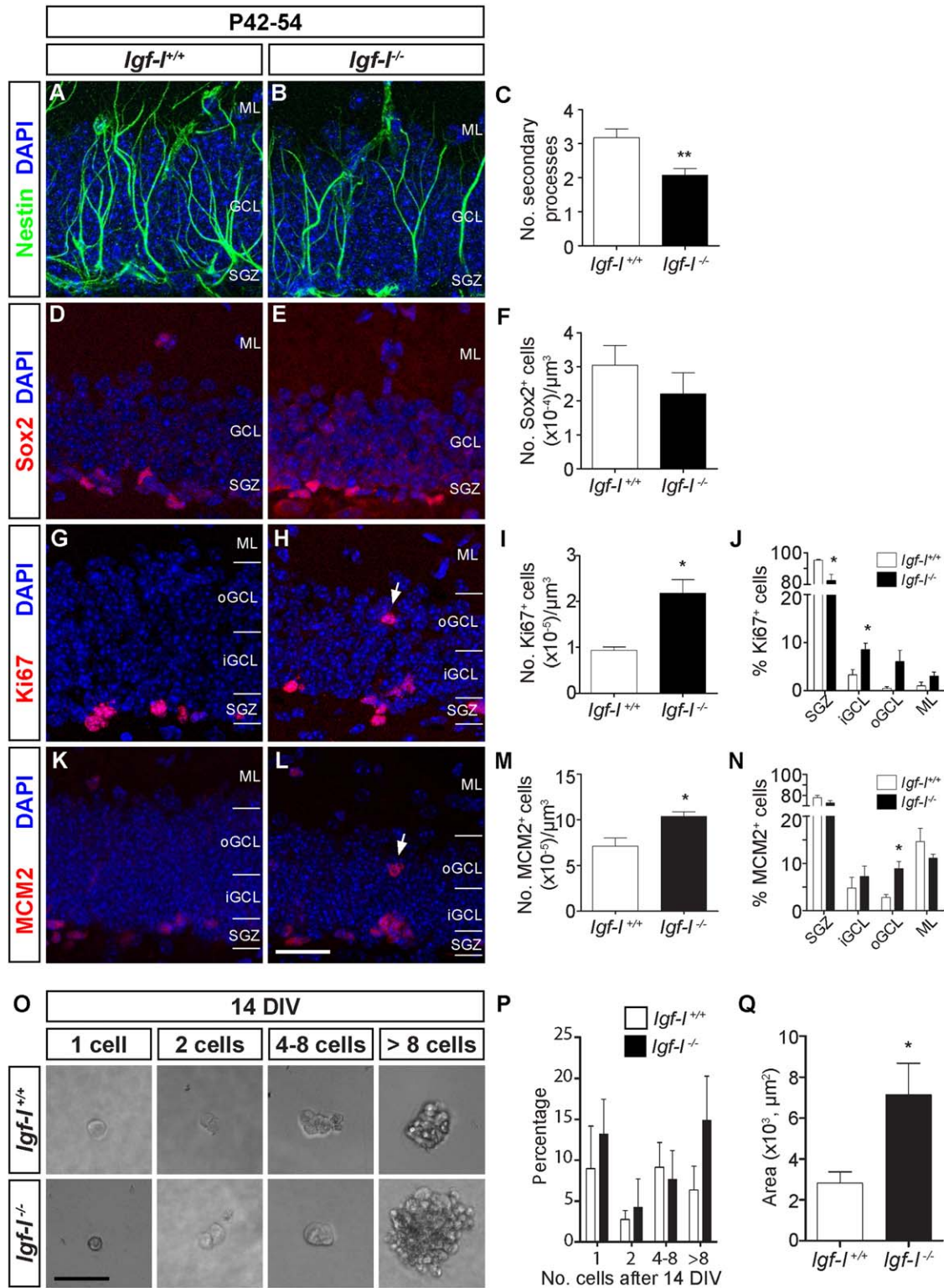


Figure 1. Effect of *Igf-1* deletion on hippocampal neural stem cells and proliferative cells. Coronal sections from P42-54 *Igf-1^{+/+}* and *Igf-1^{-/-}* mice were labeled with an anti-Nestin (A, B), anti-Sox2 (D, E), anti-Ki67 (G, H) or anti-MCM2 (K, L) antibody and counterstained with 4',6-diamidino-2-phenylindole (DAPI). All the images are z-stack projections of confocal images taken every 2 μm. The graphs show the number of secondary processes per cell in Nestin⁺-cells (C), the number of Sox2⁺-cells (F), Ki67⁺-cells (I), the distribution of the Ki67⁺-cells in the different subdivisions of the DG (J), the number of MCM2⁺-cells (M) and the distribution of the MCM2⁺ cells (N). Nestin⁺-cells had less secondary branches in *Igf-1^{-/-}* mice compared with their *Igf-1^{+/+}* littermates. The number of Ki67⁺- and MCM2⁺-cells in the DG of *Igf-1^{-/-}* mice was significantly higher than in the *Igf-1^{+/+}* mice. The Ki67⁺-cells in *Igf-1^{+/+}* animals were mainly located in the SGZ, whereas in the *Igf-1^{-/-}* mice, a decrease of Ki67⁺-cells in the SGZ and a marked increase in the inner and outer GCL was seen (arrow), where MCM2⁺-cells also located (arrow). hippocampal stem cells (HPSCs) were isolated from P21 *Igf-1^{+/+}* and *Igf-1^{-/-}* mice, and seeded as single cells for clonal analysis under low insulin conditions (O). Of the seeded single cells, some remained as single cells while others divided into cell pairs, groups of 4–8 cells or into neurospheres with more than eight cells. The graphs represent the proportions of these four different fates (P) and the neurosphere area (Q). The percentages of each category were similar in *Igf-1^{+/+}* and *Igf-1^{-/-}* cultures. The *Igf-1^{-/-}* cells formed bigger neurospheres after 14 days in culture, indicative of an increase in progenitor cell proliferation. The results are the mean ± SEM from 4–6 mice and of 9–16 neurospheres from four cultures: *, *p* < .05, **, *p* < .01, Student's *t*-test. Scale bar (L and O): 23.9 μm (A–L) and 34.69 μm (O). Abbreviations: GCL, granule cell layer; Igf-1, insulin-like growth factor-I; ML, molecular layer; SGZ, subgranular zone.

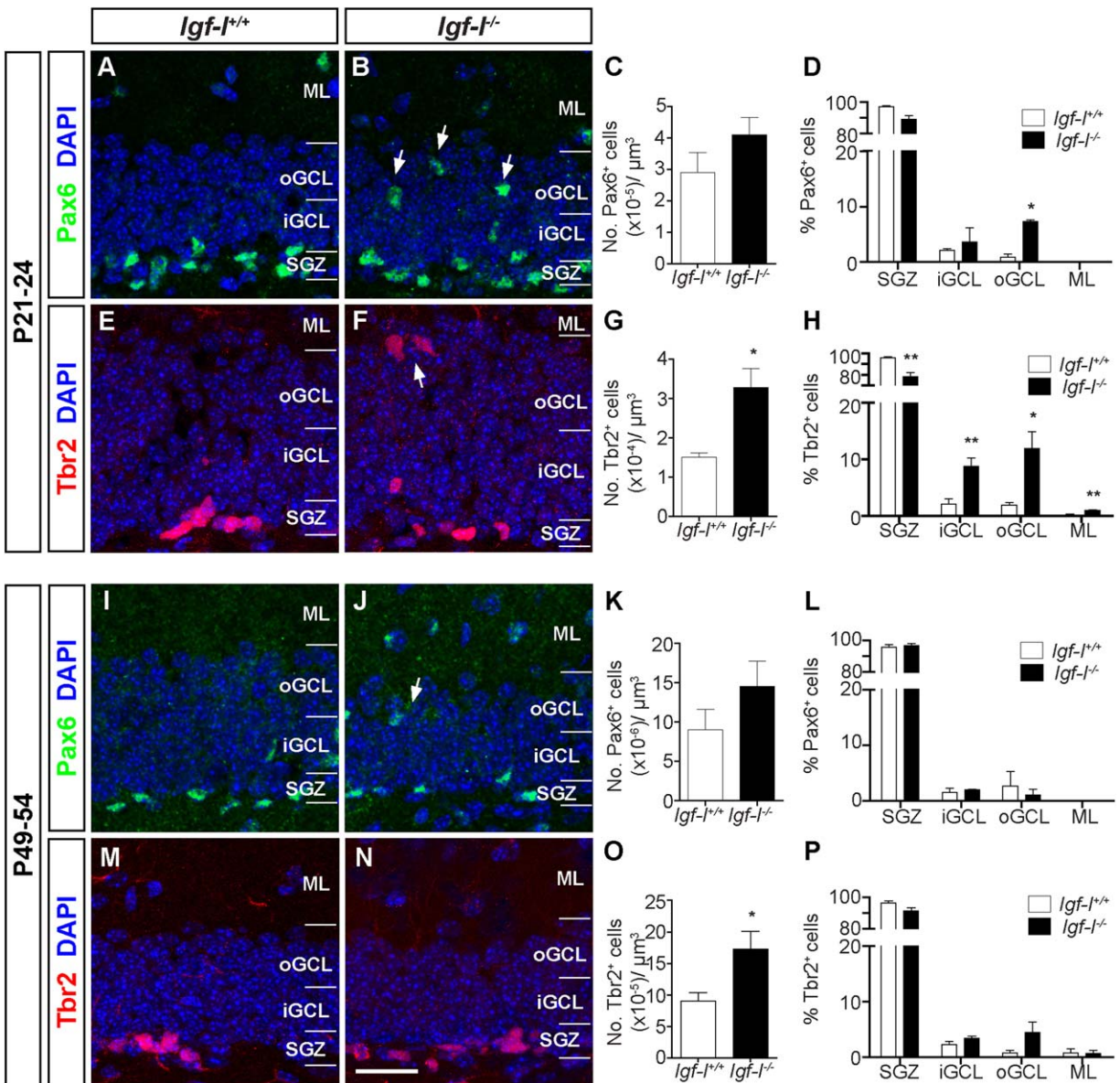


Figure 2. Increased number and altered distribution of Tbr2⁺-intermediate neuronal progenitors in the dentate gyrus of *Igf-1*^{-/-} mice. Coronal sections from P21-24 and P49-54 *Igf-1*^{+/+} and *Igf-1*^{-/-} mice were labeled with anti-Pax6 (A, B and I, J) and anti-Tbr2 (E, F and M, N) antibodies, and counterstained with DAPI. All the images are z-stack projections of confocal images. The graphs show the number of Pax6⁺-cells (C and K) and Tbr2⁺-cells (G and O), and their distribution in the subdivisions of the DG (D, H, L, and P) in *Igf-1*^{+/+} and *Igf-1*^{-/-} mice. In the *Igf-1*^{-/-} mice there was a twofold increase in the number of Tbr2⁺ neuronal progenitors. In P21 *Igf-1*^{-/-} mice, more Pax6⁺- and Tbr2⁺- cells were located in the inner and outer GCL, and in the ML, than in the *Igf-1*^{+/+} mice. The results are the mean \pm SEM from 3 to 4 mice: * $p < .05$, ** $p < .01$; Student's *t*-test. Scale bar (N): 23.9 μ m. Abbreviations: Hi, hilus; iGCL, inner granule cell layer; Igf-1, insulin-like growth factor-1; ML, molecular layer; oGCL, outer granule cell layer; SGZ, subgranular zone.

presence of truncated peptides in this KO mouse since it carries a deletion of a portion of exon 4 of the *Igf-1* gene whereas the other exons remain intact [35].

As a mouse with a complete knockout of the *Igf-1* gene is not available, we generated a riboprobe specific to the product of exon 4 and performed in situ hybridization in cryostat sections from *Igf-1*^{+/+} and *Igf-1*^{-/-} mice. *Igf-1* mRNA expression was clearly detected in cells having a relatively large body size located in the Hi and in the proximities of the SGZ (Supporting Information Fig. S2A, top). Cells in the GCL appeared also positive for *Igf-1* mRNA although at lower levels. In contrast, only a diffuse signal was seen in sections from *Igf-1*^{-/-} mouse (Sup-

porting Information Fig. S2A, bottom). Indeed, the pattern of *Igf-1* mRNA expression (Supporting Information Fig. S2A) was similar to that observed by immunostaining (Supporting Information Fig. S1A–S1G): *Igf-1* mRNA was more abundant in relatively large cells of the Hi, identified as PV-immunoreactive neurons, and also had a lighter expression in granule neurons. Overall, the in situ hybridization analysis supports the data obtained by immunostaining.

Using immunohistochemistry, IGF-IR positive cells were detected in the Hi, GCL and pyramidal cell layer (Supporting Information Fig. S1H), and we also observed IGF-IR in Prox1⁺ cells (Supporting Information Fig. S1I–S1K).

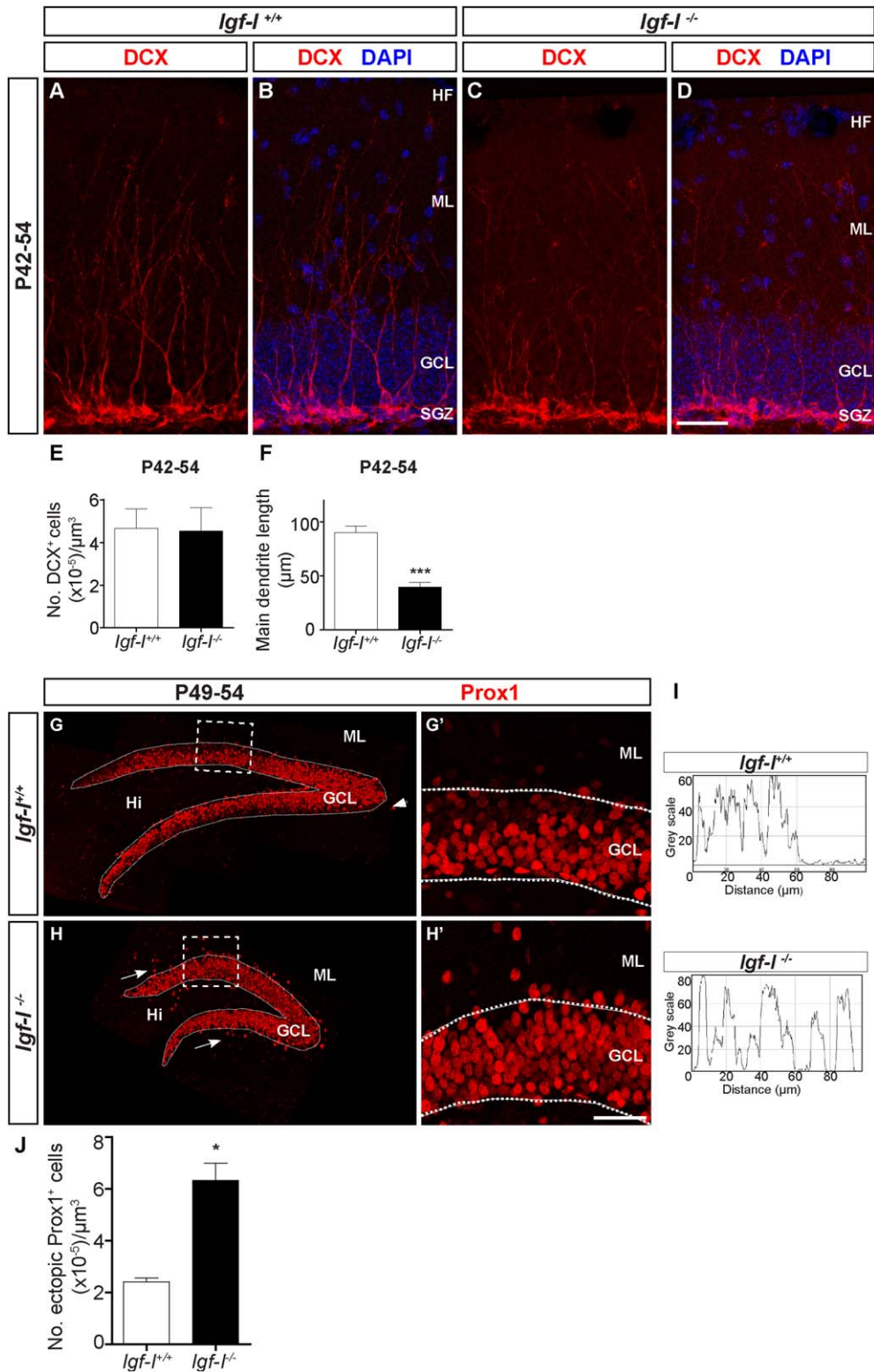


Figure 3. The lack of IGF-I alters the morphology of DCX⁺-cells and the positioning of Prox1⁺-cells in the dentate gyrus. The images show representative immunostaining for DCX (A–D) and Prox1 (G–H') in coronal sections from P42-54 *Igf-1*^{+/+} and *Igf-1*^{-/-} mice counterstained with DAPI. All the images are z-stack projections of confocal images. The graphs show the number of DCX⁺-cells per volume at P42-54 (E), the main dendrite length of DCX⁺ cells (F) and the number of Prox1⁺ cells located outside the GCL (limits indicated in the images by dotted lines) in *Igf-1*^{+/+} and *Igf-1*^{-/-} mice (J). The line plots (I) show the Prox1 fluorescence intensity from the Hi to the ML in confocal images taken from coronal sections. The dendrites in the *Igf-1*^{-/-} mice were shorter and less radially oriented than in *Igf-1*^{+/+} mice. A twofold increase in the number of ectopic Prox1⁺-cells in the DG (arrows) of *Igf-1*^{-/-} mice was found (J), although some ectopic Prox1⁺ cells were also evident in the *Igf-1*^{+/+} mice (arrowhead). The results are the mean ± SEM from 3–7 mice and 70 neurons of each genotype: *, $p < .05$, ***, $p < .001$; Student's *t*-test. Scale bar (D and H): A–D, 35.76 μm; G and H, 130.09 μm; G' and H', 31.91 μm (enlarged areas). Abbreviations: GCL, granule cell layer; HF, hippocampal fissure; Hi, hilus; Igf-I, insulin-like growth factor-I; ML, molecular layer; SGZ, subgranular zone.

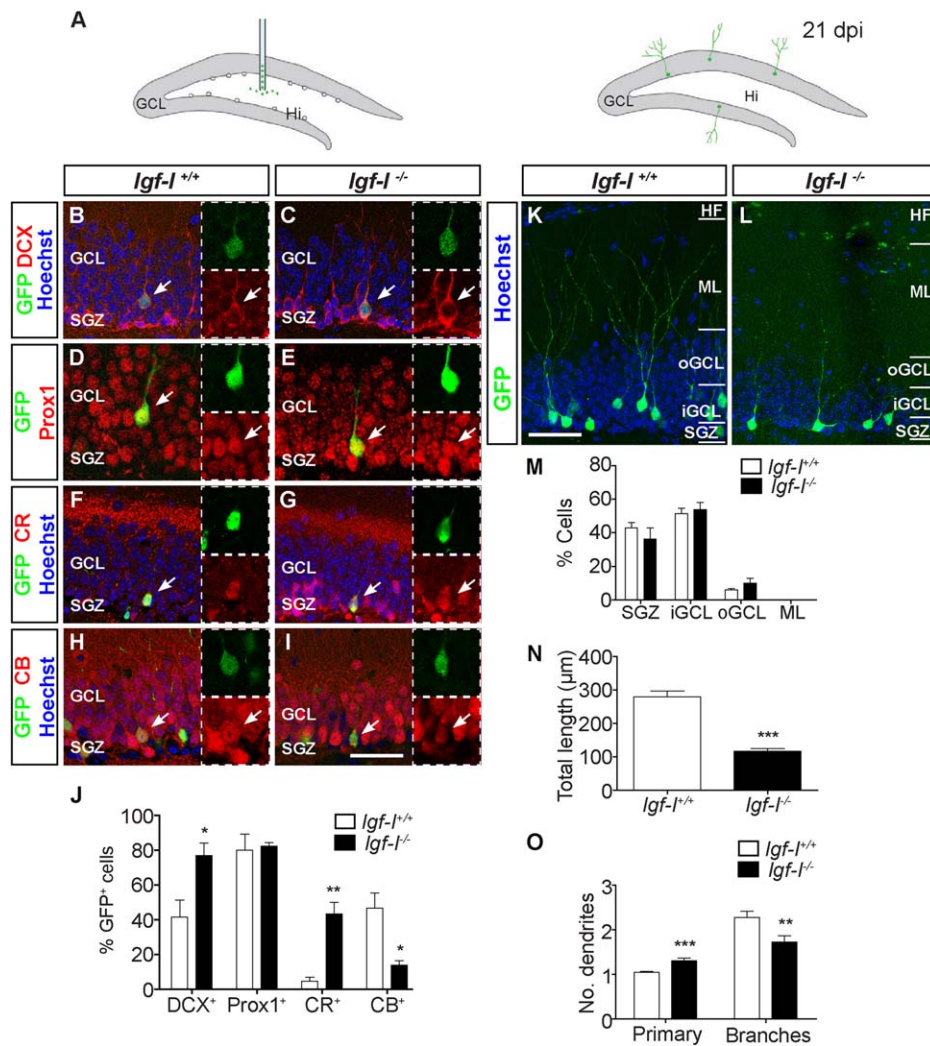


Figure 4. The differentiation of newly generated granule neurons is impaired by the lack of IGF-I. *Igf-1*^{+/+} and *Igf-1*^{-/-} mice (P21) were injected with retroviral particles in Hi of the DG to label proliferating cells and their progeny, and they were sacrificed at 21 dpi (A, scheme of experimental design). The confocal images (single plane) show the immunostaining for DCX/GFP (B, C), Prox1/GFP (D, E), CR/GFP (F, G) and CB/GFP (H, I) and the morphology and distribution of GFP⁺ cells (K, L, z-stack projections) in coronal sections from *Igf-1*^{+/+} and *Igf-1*^{-/-} mice counterstained with Hoechst. The graphs show the percentage of GFP⁺ cells expressing DCX, Prox1, CR and CB in coronal sections from *Igf-1*^{+/+} and *Igf-1*^{-/-} mice (J), the distribution of GFP⁺ cells in different subdivisions of the GCL (M), the total length of GFP⁺ cells (N), and the number of primary dendrites and dendrite branches per cell (O). The *Igf-1*^{-/-} mice had a significant increase in the percentage of GFP⁺ cells expressing DCX and CR, and a significant decrease in CB⁺ cells. GFP⁺ cells in the *Igf-1*^{-/-} mice had a more multipolar and immature morphology than in the *Igf-1*^{+/+} mice. The results are the mean ± SEM of 95–100 cells from 3 to 4 mice. *, *p* < .05, **, *p* < .01, ***, *p* < .001, Student's *t*-test. Scale bar (I and K): B–I, 44 μm (29.6 μm, insets); K, L, 56.2 μm. Abbreviations: Hi, hilus; HF, hippocampal fissure; Igf-1, insulin-like growth factor-I; iGCL, inner granule cell layer; ML, molecular layer; oGCL, outer granule cell layer; SGZ, subgranular zone.

Our in situ hybridization and immunohistochemistry techniques did not allow us to unambiguously determine whether *Igf-1* was expressed in NSCs and progenitors from histological sections. However, we found specific expression of *Igf-1* mRNA in HPSCs isolated from *Igf-1*^{+/+} mice, whereas *Igf-1* was not detected in cells from *Igf-1*^{-/-} mice (Supporting Information Fig. S2B). *Igf-1r* mRNA was expressed by HPSCs, with no significant differences in *Igf-1*^{+/+} and *Igf-1*^{-/-} cells (Supporting Information Fig. S1C). As seen in the graphs (Supporting Information Fig. S1D–S1E) the levels of both growth factor and its receptor tended to increase from HPSC proliferation to differentiation but the observed changes were not statistically significant ($p = 0.15–0.85$).

In conclusion, the expression of IGF-I and IGF-IR in NSCs and neurons suggests that the local production of this growth factor may regulate the formation of granule cells from their progenitors in the postnatal/adult DG.

The Stage-Specific Roles of IGF-I During Hippocampal Neurogenesis

To analyse the role of IGF-I in hippocampal neurogenesis, first, we used a global *Igf-1* KO mouse [35]. These mice do not express *Igf-1* in the HP as mentioned above. Furthermore, they have extremely low levels of serum IGF-I compared to *Igf-1*^{+/+} [58] and suffer a 3.5-fold decrease in their body weight (Supporting Information Table S4, see also [12, 24, 25,

35, 36, 59]). Here we found a 0.67-fold and 2.4-fold reduction in the estimated volume of the HP in *Igf-1*^{-/-} compared to the *Igf-1*^{+/+} mice at P21 and P49, respectively, with similar changes in the CA, DG and GCL (Supporting Information Table S5). In contrast, the decrease in the volume of the OB was similar at both ages (3.3-fold) and of the same magnitude to the reduction of body weight.

In the light of these data, and given the expression of IGF-I and its receptor in the DG, we studied the role of IGF-I during late postnatal/adult hippocampal neurogenesis in depth, using specific antibodies against proliferative cells, NSCs, intermediate neuronal progenitor cells, neuroblasts and

neurons. Furthermore, we used microdissected tissue, in vivo BrdU labelling, NSC cultures and the injection of retroviral particles into the DG of *Igf-1*^{+/+} and *Igf-1*^{-/-} mice to label proliferative cells, and to analyze the molecular and morphological differentiation of newly formed neurons in vivo. Finally, we studied the role of local IGF-I in neurogenesis by analyzing a nervous system specific *Igf-1* conditional KO mouse.

Effect of *Igf-1* Deletion on Hippocampal Stem Cells and Cycling Cells In Vivo

To evaluate the effect of the lack of IGF-I in NSCs, we labeled sections from P42-54 *Igf-1*^{+/+} and *Igf-1*^{-/-} mice with antibodies against Nestin, a marker of RGCs [60], and Sox2, a transcription factor detected in adult NSCs [61] (Fig. 1A–1F). In the *Igf-1*^{-/-} mice Nestin⁺-cells were evident in the DG, albeit with a significant reduction in the number of secondary processes compared to *Igf-1*^{+/+} animals ($p < .01$, Fig. 1A–1C). In contrast, a similar number of Sox2⁺-cells was found in both mouse types ($p = .35$; Fig. 1D–1F).

To study the role of *Igf-1* deletion on proliferative cells, we analyzed the number of Ki67⁺- and MCM2⁺-cells [62, 63] in sections from P49 mice (Fig. 1G–1N). Ki67⁺-cells were mainly located in the SGZ of *Igf-1*^{+/+} mice (Fig. 1G–1J), while in the *Igf-1*^{-/-} there were more Ki67⁺-cells (twofold increase, $p < .05$, Fig. 1H–1I) and their distribution in the DG was distinct to that in the *Igf-1*^{+/+}. Thus, in the *Igf-1*^{-/-} mice there were 13.6% fewer Ki67⁺-cells in the SGZ ($p < .05$) yet 2.5-fold more of these cells were in the iGCL. We also quantified a 12.7-fold and a 3.1-fold increase in Ki67⁺-cells in the oGCL and in the ML, respectively, although these changes were not significant ($p = .1$; Fig. 1J). In addition, the *Igf-1*^{-/-} mice had a higher number of MCM2⁺-cells (1.31-fold, $p < .05$, Fig. 1K–1M) some of which were displaced in the oGCL (3.1-fold increase, $p < .005$, Fig. 1K–1L, 1N). These results show that in the absence of IGF-I, there is an increase in the number of cycling cells and their position in the GCL is altered.

The Lack of IGF-I Promotes the Proliferation of HPSCs in Clonal Analysis

To further explore the impact of *Igf-1* KO on cell proliferation, HPSCs were grown as neurospheres under population

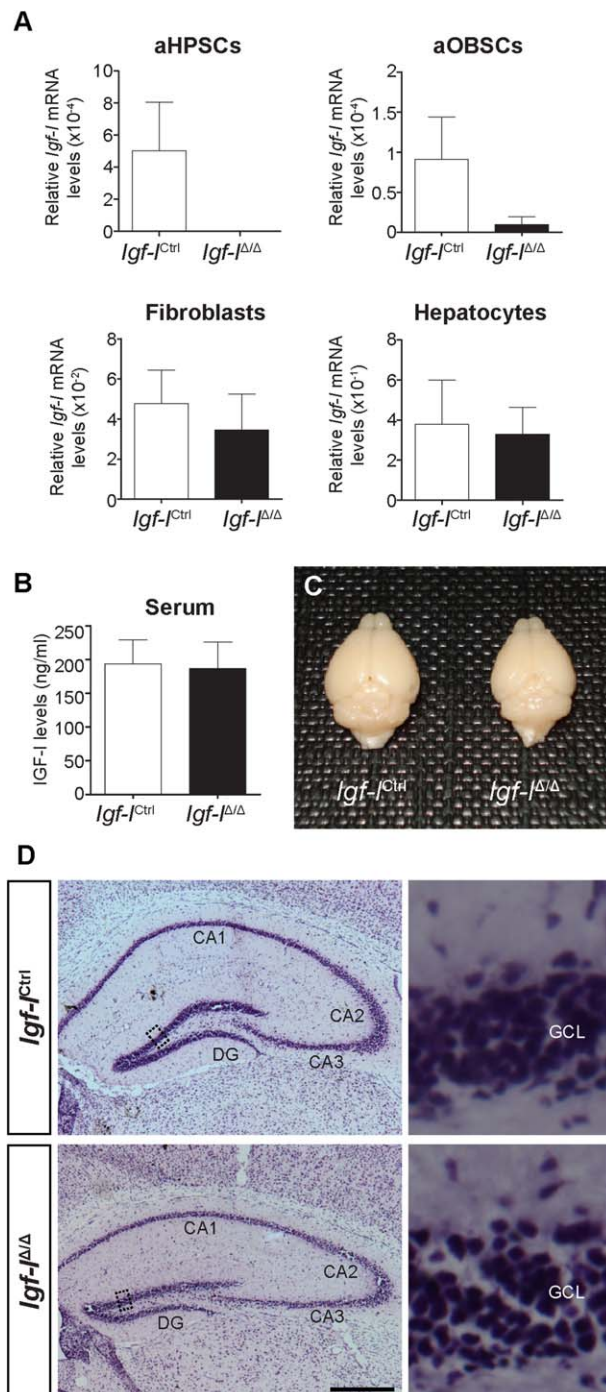


Figure 5. Generation and characterization of a conditional *Igf-1* KO specific to the nervous system. *Igf-1* loxP mice and Nestin-Cre mice were crossed to generate a conditional *Igf-1* KO mice in which *Igf-1* is deleted only in neural cells. The graphs (A) represent the relative *Igf-1* mRNA levels in aHPSCs, aOBSCs, fibroblasts, and hepatocytes from 2 to 20 month-old *Igf-1*^{Ctrl} and *Igf-1*^{Δ/Δ} measured by RT-qPCR. The graph (B) shows similar IGF-I levels in serum from *Igf-1*^{Ctrl} and *Igf-1*^{Δ/Δ} mice measured by ELISA. The expression of *Igf-1* was abolished completely or reduced to very low levels in cells from neural tissues in the *Igf-1*^{Δ/Δ} mice, whereas it was similar to the *Igf-1*^{Ctrl} in cells from nonneural tissues. The results are the mean \pm SEM from 3 to 4 mice. (C) The images show the normal gross brain structure of P49 *Igf-1*^{Ctrl} and *Igf-1*^{Δ/Δ} mice. (D) Coronal sections from P49 *Igf-1*^{Ctrl} and *Igf-1*^{Δ/Δ} mice stained with cresyl violet revealed that the GCL in the *Igf-1*^{Δ/Δ} mice was less compacted compared with that of the *Igf-1*^{Ctrl} mice. Scale bar (D): C, 8.2 mm; D, 367 μ m (enlarged areas, 21 μ m). Abbreviations: aHPSCs, adult hippocampal stem cells; aOBSCs, adult olfactory bulb stem cells; CA1, CA2 and CA3, Cornu ammonis1, 2 and 3; DG, dentate gyrus; GCL, granule cell layer; Igf-1, insulin-like growth factor-I.

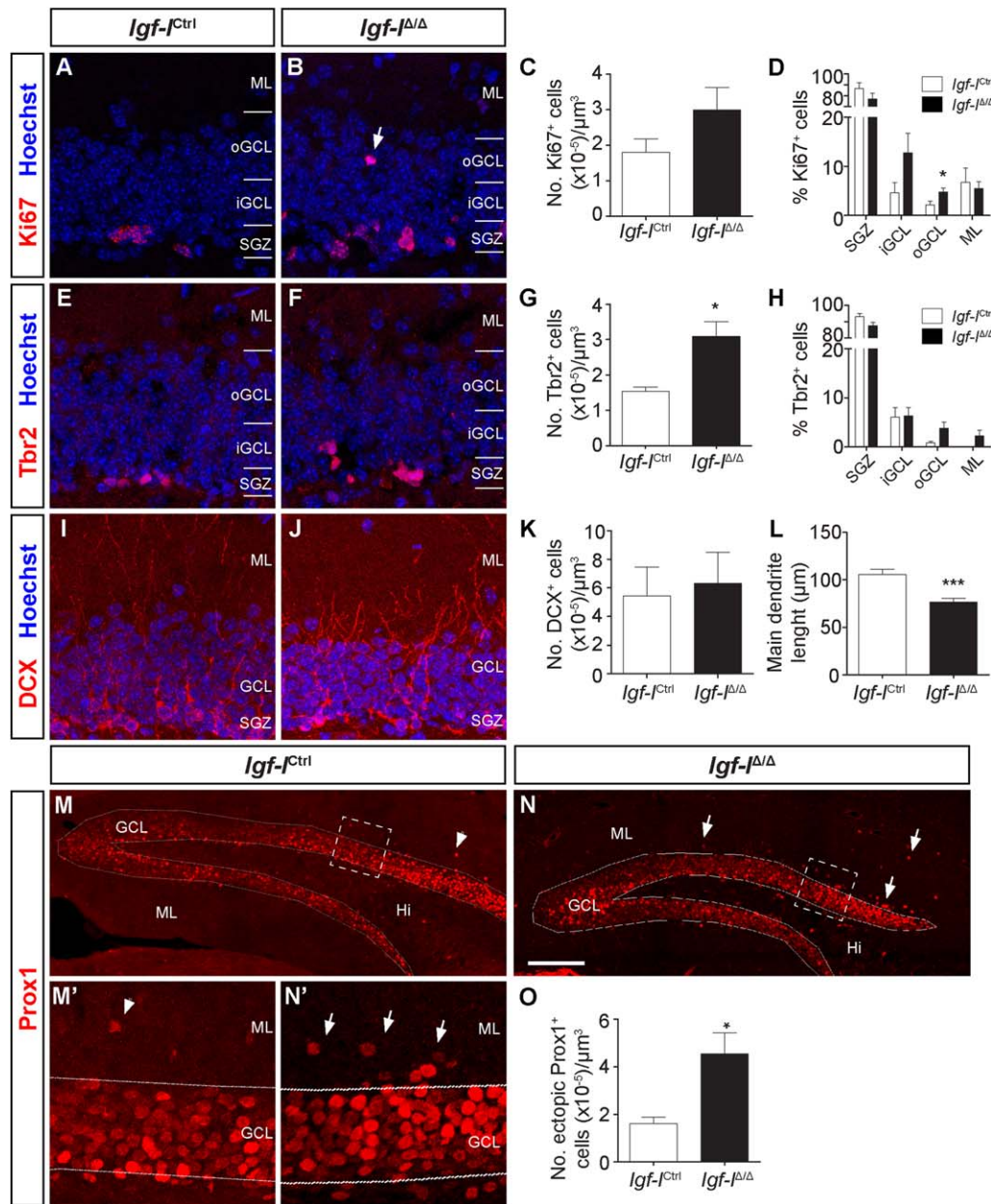


Figure 6. A nervous system-specific *Igf-1* deletion impairs postnatal/adult hippocampal neurogenesis. Coronal sections from P49 *Igf-1^{Ctrl}* and *Igf-1^{Δ/Δ}* mice labeled with an anti-Ki67 (A, B), anti-Tbr2 (E, F), anti-DCX (I, J) and anti-Prox1 (M, N, mosaic images; M'–N', enlarged areas) antibodies and counterstained with Hoechst. All the fluorescent images are z-stack projections of confocal images taken every 2 μm. The graphs represent the number of Ki67⁺-cells (C), Tbr2⁺-cells (G), DCX⁺-cells (K) and ectopic Prox1⁺-cells (O); the distribution of Ki67⁺-cells (D) and Tbr2⁺-cells (H) in the subdivisions of the DG and the main dendrite length of DCX⁺-cells (L). The *Igf-1^{Δ/Δ}* mice presented higher number of Tbr2⁺-cells and ectopic Prox1⁺-cells and shorter and less radially oriented DCX⁺ cells in the DG compared with the *Igf-1^{Ctrl}* mice. Arrows indicate Ki67⁺-cells and ectopic Prox1⁺-cells in *Igf-1^{Δ/Δ}* mice and arrowheads show ectopic Prox1⁺-cells in the *Igf-1^{Ctrl}* mice. The results are the mean ± SEM from 4 to 5 mice and 39 neurons of each genotype: *, $p < .05$, ***, $p < .001$, Student's t-test. Scale bar (P): 29.1 μm (A–J); 125 μm (M, N); 29.1 μm (M'–N'). Abbreviations: GCL, granule cell layer; Hi, hilus; iGCL, inner granule cell layer; *Igf-1*, insulin-like growth factor-1; ML, molecular layer; oGCL, outer granule cell layer; SGZ, subgranular zone.

conditions. After dissociating the neurospheres, the percentage of cells in each phase of the cell cycle was determined by flow cytometry using Propidium iodide (PI). The HPSCs from *Igf-1^{-/-}* and *Igf-1^{+/+}* mice had the same percentages of cells in each phase (G₀/G₁: *Igf-1^{+/+}*, 78.6 ± 4.9, *Igf-1^{-/-}*, 80.7 ± 3.0; S: *Igf-1^{+/+}*, 9.7 ± 2.5, *Igf-1^{-/-}*, 9.7 ± 2.3; G₂/M: *Igf-1^{+/+}*, 11.7 ± 2.4, *Igf-1^{-/-}*, 9.6 ± 1.4; $n = 3-4$).

We also studied the effect of the lack of IGF-I on HPSC self-renewal and proliferation by clonal analysis (Fig. 10). The number of wells containing one single cell the day after seeding was similar in both genotype cultures (*Igf-1^{+/+}*, 45.5 ± 1.8; *Igf-1^{-/-}*, 32.3 ± 7.4; $n = 4$), and 28.7% of the *Igf-1^{+/+}* single cells and 39.8% of the *Igf-1^{-/-}* single cells ($p = .36$) survived for 14 days and generated clones or remained

as single cells. The clones were classified in groups depending on the number of cells they contained (2, 4–8 or >8 cells). After 14 DIV, we found the same percentage of single cells and clones in cultures from both genotypes (Fig. 1P). However, the size of neurospheres, i. e., groups of more than eight cells [55], was larger in *Igf-1*^{-/-} than *Igf-1*^{+/+} cultures (2.5-fold, $p < .05$; Fig. 1Q). The results suggest that the absence of IGF-I did not alter the ability of HPSCs to self-renew in this assay, although the proliferation of progenitor cells was enhanced.

The Lack of IGF-I Disrupts the Number and Position of Progenitor Cells in the DG

In the DG, the Pax6 transcription factor is expressed by NSCs and in progenitors that have not yet been specified to generate neurons or glia [6, 64]. In P21–24 mice, there was 1.29-fold more Pax6⁺-cells in *Igf-1*^{-/-} animals compared to *Igf-1*^{+/+} mice, although this change was not significant ($p = .21$, Fig. 2A–2C). Although Pax6⁺-cells were located primarily in the SGZ in *Igf-1*^{-/-} and *Igf-1*^{+/+} mice, we found 8.3-fold more Pax6⁺-cells in the oGCL of *Igf-1*^{-/-} animals ($p < .05$, Fig. 2A, 2B, 2D). By contrast, no statistically significant differences were detected in P49–54 *Igf-1*^{-/-} mice (Fig. 2I–2L). Additionally, in these older mice, there were fewer (2.7 to 3.3-fold) Pax6⁺-cells than in younger animals (P21) in both mouse genotypes.

Tbr2 is expressed in the intermediate neuronal progenitor cells; probably those committed toward the neuronal lineage [6, 64, 65]. In P21–24 animals, we observed a twofold increase in the number of Tbr2⁺-cells in the *Igf-1*^{-/-} compared to the *Igf-1*^{+/+} mice ($p < .05$, Fig. 2E–2G). Furthermore, higher percentages of Tbr2⁺-cells were detected in the iGCL, oGCL and ML of the *Igf-1*^{-/-} animals ($p < .05$ and $p < .01$), whereas there was a lower percentage of Tbr2⁺-cells in the SGZ ($p < .01$; Fig. 2E, 2F, 2H) compared to that in the *Igf-1*^{+/+} mice. This accumulation of Tbr2⁺ cells persisted in P49–54 *Igf-1*^{-/-} mice (1.8-fold increase, $p < .05$; Fig. 2M–2O) yet there were no significant changes in their distribution (Fig. 2P). Additionally, in P49–54 animals there was a decrease (1.7 to 1.9-fold) in the number of Tbr2⁺-cells compared to that of P21–23 mice.

In summary, the altered number and/or distribution of Pax6⁺- and Tbr2⁺-cells suggests that in the absence of IGF-I, the transition of progenitor cells to the next stage of neurogenesis is disrupted.

Altered Morphology of DCX⁺-Cells and Misplacement of Prox1⁺-Neurons in *Igf-1*^{-/-} Mice

DCX is a microtubule associated protein that is expressed in neuroblasts and immature neurons [66]. In P21–24 mice, there was less DCX labeling in *Igf-1*^{-/-} mice than in the *Igf-1*^{+/+} animals (Supporting Information Fig. S3A–S3D). In older mice (P42–54), while the number of DCX⁺-cells in *Igf-1*^{+/+} and *Igf-1*^{-/-} mice was similar, these cells had a less radial morphology in the *Igf-1*^{-/-} than in the *Igf-1*^{+/+} mice (Fig. 3A–3E). Indeed, the dendritic tree of DCX⁺-cells occupied the entire width of the ML in *Igf-1*^{+/+} mice, while DCX⁺-dendrites in the *Igf-1*^{-/-} often failed to reach the ML. This difference is exemplified by the DCX⁺-cells having a 2.3-fold shorter main dendrite in *Igf-1*^{-/-} animals ($p < .001$; Fig. 3F).

Differentiated granule neurons are characterized by the expression of the homeobox transcription factor, Prox1 [45, 46]. In *Igf-1*^{+/+} mice, Prox1⁺-cells were virtually restricted to the GCL at P21–24 and P49–54, although scattered cells were detected outside of the GCL (arrowhead in Supporting Information Fig. S3E; Fig. 3G). However, the distribution of Prox1⁺-cells was not well defined in *Igf-1*^{-/-} mice, forming a more disorganized GCL (Supporting Information Fig. S3F; Fig. 3H). To determine the contour of the GCL, we measured the fluorescence intensity of Prox1⁺-cells from the Hi to the ML in confocal images. In the resulting line plots, the fluorescence signal in *Igf-1*^{+/+} mice was grouped into a narrow area that possibly corresponds to the SGZ and GCL ($\approx 60 \mu\text{m}$), whereas in the *Igf-1*^{-/-} mice we detected other fluorescence peaks due to ectopic cells (Fig. 3I). To quantify this disorganization, we delineated the GCL and counted the Prox1⁺-cells outside this area in the ML and Hi. We found a 3.2-fold increase in the number of ectopic Prox1⁺-cells in P21–24 *Igf-1*^{-/-} mice ($p < .05$; Supporting Information Fig. S3G). Similarly, the P49–54 *Igf-1*^{-/-} animals exhibited a 2.8-fold increase in the number of Prox1⁺-cells located outside the GCL ($p < .05$, Fig. 3J).

Finally, we ruled out that the observed effects in the *Igf-1*^{-/-} mice were due to a process of reactive gliosis, inflammation or cell death. We performed immunohistochemistry with an antibody against S100 β to label mature astrocytes, or Iba1 to label microglia, and no apparent differences were observed between *Igf-1*^{+/+} and *Igf-1*^{-/-} mice (unpublished observations). Cell death was studied by TUNEL labeling and with an antibody against activated caspase 3, yet we failed to detect apoptotic cells in our sections (unpublished observations). Additionally, we analyzed cell death by flow cytometry of HPSCs labeled with Annexin V and PI, and we observed no significant differences in the percentage of dead cells in HPSCs from *Igf-1*^{-/-} and *Igf-1*^{+/+} mice (early apoptosis: *Igf-1*^{+/+} 6.4 ± 2.5 , *Igf-1*^{-/-} 7.0 ± 3.0 ; late apoptosis: *Igf-1*^{+/+} 28.3 ± 4.0 , *Igf-1*^{-/-} 33.3 ± 5.2 ; dead: *Igf-1*^{+/+} 14.1 ± 2.1 , *Igf-1*^{-/-} 13.7 ± 3.0 ; $n = 4$).

Altogether, our results show that the lack of IGF-I alters the morphology of RGCs, and it causes an accumulation and displacement of cycling cells in the GCL, partially due to the increase of neuronal progenitors. Moreover, *Igf-1* deletion impairs the morphology of DCX⁺-cells, and the migration/positioning of Prox1⁺-neurons in the GCL.

Altered Molecular and Morphological Differentiation of Newly Generated Neurons in *Igf-1*^{-/-} Mice

We studied the effect of *Igf-1* deletion on the formation of granule neurons in a restricted time window (from P21 to P42). We injected EGFP-expressing retroviral particles into *Igf-1*^{+/+} and *Igf-1*^{-/-} P21 mice (Fig. 4A), to label proliferating cells and analyze the differentiation-maturation and position of the newly formed neurons in the GCL [7]. We did not find statically significant differences in the number of GFP⁺-cells between the animals at 21 dpi (*Igf-1*^{+/+} 231.0 ± 133.1 , *Igf-1*^{-/-} 80.25 ± 31.48 ; $n = 4$, $p = .35$). However, the *Igf-1*^{-/-} mice had a 1.8-fold more GFP⁺-cells expressing DCX than in the *Igf-1*^{+/+} mice ($p < .05$, Fig. 4B, 4C, 4J), while the percentage of GFP⁺-cells expressing Prox1 was similar in animals of both genotypes ($\approx 80\%$, Fig. 4D, 4E, 4J). To better characterize the degree of granule neuron differentiation-maturation, we used antibodies against CR which can be detected when DCX

expression decreases and CB which is detected after CR expression [6, 64]. There was a 9.2-fold increase in the percentage of GFP⁺-cells expressing CR in *Igf-1*^{-/-} mice ($p < .01$, Fig. 4F, 4G, 4J) and a 3.3-fold decrease in the percentage of GFP⁺-cells expressing CB compared with the *Igf-1*^{+/+} mice ($p < .05$, Fig. 4H, 4I, 4J). By contrast, we did not find any GFP⁺-cells positive for S100 β , Ki67 or Iba1 in mice of either genotype (unpublished observations).

The distribution of GFP⁺-cells in the GCL was similar in both mouse genotypes (Fig. 4K, 4L, 4M). However, the GFP⁺-cells in *Igf-1*^{-/-} mice had a more immature morphology than in the *Igf-1*^{+/+} animals, as reflected by a 2.4-fold reduction in the total length of the dendrites ($p < .001$) and a 1.24-fold increase in the number of primary dendritic branches ($p < .001$), as well as a 1.25-fold decrease in secondary branches ($p < .01$; Fig. 4K, 4L and N-O). Thus, the absence of IGF-I inhibits the molecular and morphological differentiation and maturation of newly formed granule cells in the postnatal/adult DG. The results also suggest a failure for the cells to polarize in the absence of IGF-I.

Brain-Derived IGF-I Affects Postnatal/Adult Hippocampal Neurogenesis

A role for locally-produced IGF-I in adult hippocampal neurogenesis has been proposed but not yet demonstrated in vivo [12, 14, 24, 32–34, 67]. The expression of *Igf-1* mRNA in the DG (Supporting Information Fig. S2) supports but does not prove this idea. To address this fundamental question we crossed *Igf-1* loxP and Nestin-Cre mice [38, 39, 41] (Supporting Information Fig. S4) to obtain mice in which *Igf-1* was deleted only in neural cells (conditional *Igf-1* KO termed as *Igf-1* ^{Δ/Δ}) and mice in which *Igf-1* expression was not altered (control mice termed as *Igf-1*^{ctrl}) (Fig. 5; Supporting Information Fig. S5). We measured *Igf-1* mRNA in two pure populations of neural cells (aHPSCs and aOBSCs) from *Igf-1*^{ctrl} and *Igf-1* ^{Δ/Δ} mice by RT-qPCR (Fig. 5A) to avoid contamination of mRNA from nonneural cells and from the vasculature. RT-qPCR analysis was also performed in fibroblasts and hepatocytes from the same mice. Levels of IGF-I protein in serum were measured by ELISA (Fig. 5B). As observed in the figures, the expression of *Igf-1* was abolished in aHPSCs from *Igf-1* ^{Δ/Δ} mice and was almost absent (a reduction of 11-fold) in aOBSCs (Fig. 5A). In contrast, the levels of *Igf-1* mRNA in fibroblasts and hepatocytes as well as the serum IGF-I levels in *Igf-1* ^{Δ/Δ} mice were similar to those in *Igf-1*^{ctrl} mice. These results show that the *Igf-1* deletion is specific to neural cells and it does not change the peripheral production of IGF-I.

Next, we analyzed the macroscopic phenotypes of the Nestin-Cre:*Igf-1* mice (Supporting Information Fig. S5C). The *Igf-1* ^{Δ/Δ} mice had a similar body weight compared to the *Igf-1*^{ctrl} mice (*Igf-1*^{ctrl}, 16.30 \pm 1.14 n = 7; *Igf-1* ^{Δ/Δ} , 15.04 \pm 0.78 n = 6; p = .396) and we did not find statistical differences in the volume of any brain area studied, except in the volume of the OB and in the GCL of the DG (Fig. 5C, 5D; Supporting Information Table S6). In fact, we found a 1.9-fold decrease in the volume of the GCL ($p < .01$) and a less compact organization of the granule neurons in this area of *Igf-1* ^{Δ/Δ} mice compared with the *Igf-1*^{ctrl} mice (Fig. 5D).

We immunostained sections from P49 *Igf-1*^{ctrl} and *Igf-1* ^{Δ/Δ} mice with antibodies against Ki67, Tbr2, DCX and Prox1 as they label the most affected cell populations in the global *Igf-*

I KO mice. The total number of Ki67⁺-cells was 1.4-fold higher in the *Igf-1* ^{Δ/Δ} mice (p = .14) although the number of those cells located in the oGCL was 2.2-fold greater ($p < .05$) in the *Igf-1* ^{Δ/Δ} mice (Fig. 6A–6D). In addition, the *Igf-1* ^{Δ/Δ} mice had a twofold increase in the number of Tbr2⁺-cells ($p < .05$) some of which were present in the oGCL and in the ML, whereas in the *Igf-1*^{ctrl} mice the Tbr2⁺-cells were rarely found in these subdivisions (Fig. 6E–6H). The main dendrite length of DCX⁺-cells in *Igf-1* ^{Δ/Δ} mice was a 1.3-fold shorter than in the *Igf-1*^{ctrl} mice ($p < .001$) and the dendrites were oriented less radially to the SGZ, without being affected the number of DCX⁺-cells (Fig. 6I–6L). Moreover, the *Igf-1* ^{Δ/Δ} mice showed a twofold increase in the number of ectopic Prox1⁺-cells compared with the *Igf-1*^{ctrl} mice ($p < .05$, Fig. 6M–6O). All these results show that the *Igf-1* ^{Δ/Δ} mice have a similar phenotype in the GCL to the global *Igf-1* KO mice.

To further analyse the molecular mechanisms underlying the IGF-I effect, we isolated HPSCs from *Igf-1*^{ctrl} and *Igf-1* ^{Δ/Δ} mice and we maintained them as floating neurospheres adding FGF-2 and EGF every 3 days (“experimental design 1”) [48]. After 6 DIV, we analysed the expression of genes involved in self-renewal, cell proliferation, differentiation, cell death and cell signaling by RT-qPCR (Fig. 7A–7C; Supporting Information Fig. S6A, Table S3). We found a 2.7-fold, 1.9-fold, and 2.7-fold increase (in log₂ scale) in the mRNA levels of *Hes5*, *Ngn2*, and *Dscaml1*, respectively, as well as a 1.8-fold decrease in *Calb1* in cells from *Igf-1* ^{Δ/Δ} mice compared with cells from *Igf-1*^{ctrl} mice (Fig. 7B). When we compared the raw mRNA values in linear scale we found a 7-fold, 2.9-fold, 5.7-fold significant increases in *Hes5*, *Ngn2*, and *Dscaml1* ($p < .05$) and a 3.4-fold reduction in *Calb1* ($p < .05$) (Fig. 7C). Except for S100 β , changes in all other transcripts (including *Igf1r* and *Insr*) were less than onefold in log 2 scale (Fig. 7B; Supporting Information Fig. S6A, Table S3). To determine the expression of *Hes5* and *Ngn2* mRNAs in an in vivo-ex vivo approach we dissected out the GCL-ML from adult *Igf-1*^{ctrl} and *Igf-1* ^{Δ/Δ} mouse HP, followed by RNA extraction and RT-qPCR analysis (Fig. 7D). The mRNA levels of *Hes5* and *Ngn2* were 2.2-fold and 1.5-fold (in log₂ scale) and 4.7-fold and 2.8-fold (in linear scale) greater in the GCL-ML of *Igf-1* ^{Δ/Δ} mice compared to *Igf-1*^{ctrl}. Although these increases did not reach statistical significance (p = .26 and p = .12) they were relatively similar to those obtained in HPSC cultures from *Igf-1* ^{Δ/Δ} mice. As expected, the level of *Igf-1* mRNA in the *Igf-1* ^{Δ/Δ} GCL-ML dropped sharply (6.9-fold; $p < .001$) (Fig. 7D).

Next, to analyze the percentage of cycling cells and the cell cycle exit, neurospheres were given a pulse of 5 μ M BrdU 22 hours. The dissociated cells were then cultured for 1 DIV to induce differentiation (“experimental design 2”, Fig. 7E). The quantification revealed a significantly higher percentage of Ki67⁺-cells (1.15-fold; $p < .001$) and fewer cells (1.25-fold; $p < .05$) exiting the cell cycle in *Igf-1* ^{Δ/Δ} cultures (Fig. 7F, 7G). We then studied whether the *Igf-1* conditional deletion affected cell cycle exit in vivo by performing double BrdU/Ki67 immunostaining of sections from adult mouse previously injected with BrdU. The results show a 36% reduction (p = .39; nonstatistically significant) in cells exiting the cell cycle in the *Igf-1* ^{Δ/Δ} mice in vivo.

These findings indicate that the lack of brain IGF-I impairs hippocampal neurogenesis (Supporting Information Fig. S6B) promoting the expression of *Hes5* and *Ngn2* [6, 68–70] and of

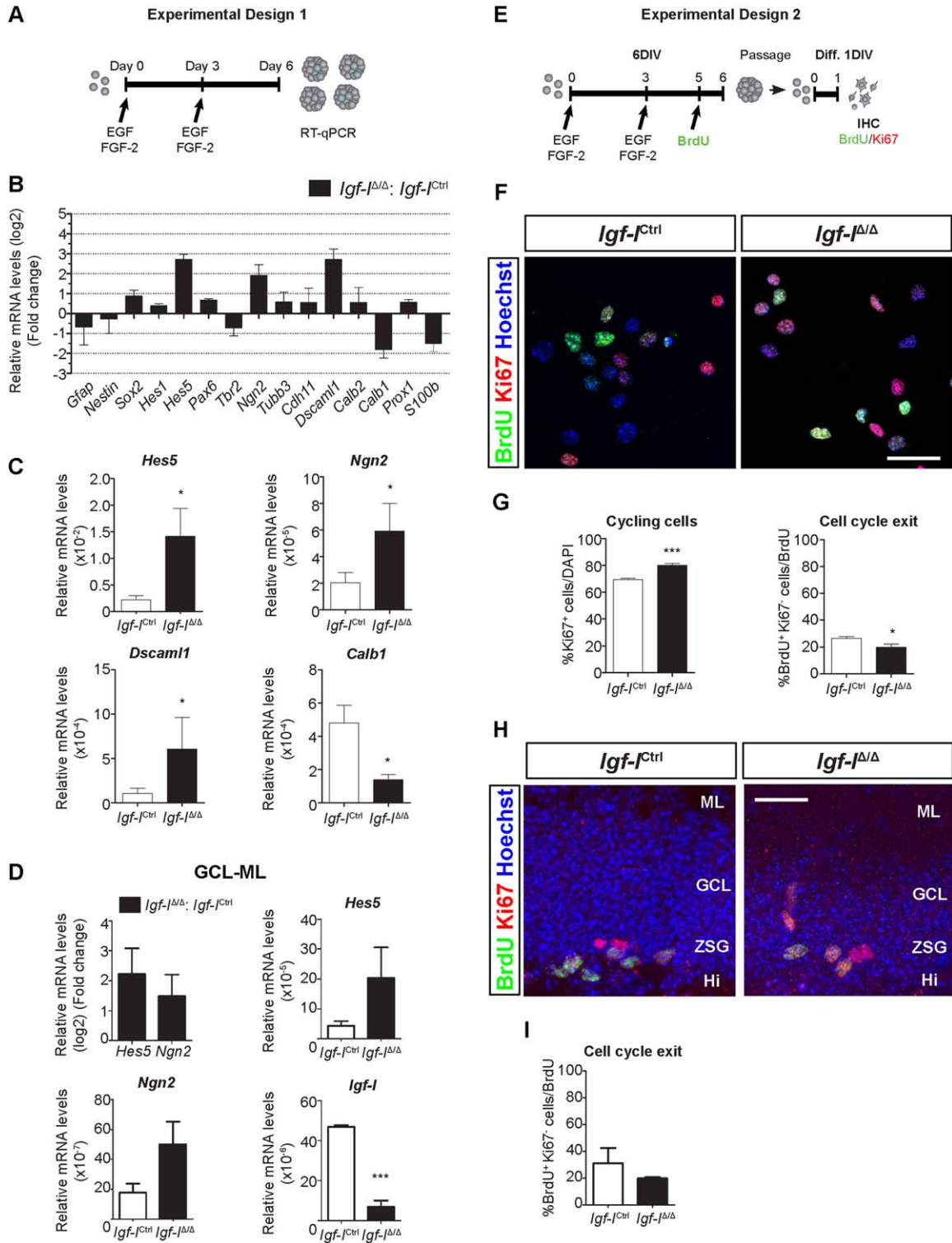


Figure 7. Effect of the lack of IGF-I in neural cells on gene expression profile and cell cycle exit. **(A)** adult HPSC (aHPSC) neurospheres from 6 months-old *Igf-1^{Ctrl}* and *Igf-1^{Δ/Δ}* mice were maintained as floating neurospheres during 6 DIV adding FGF-2 and EGF every three days, a condition that induces the initiation of differentiation in proliferating NSCs. Then, gene expression was quantified by real-time qPCR. **(B)** We found a 2.7-fold, 1.9-fold and 2.7-fold increases in the mRNA levels of *Hes5*, *Ngn2*, and *Dscam1*, respectively, as well as a 1.8-fold decrease in *Calb1* (all in \log_2 scale) in cells from *Igf-1^{Δ/Δ}* mice compared with *Igf-1^{Ctrl}* cells. **(C)** The analysis of the raw mRNA values in linear scale revealed a 7-fold, 2.9-fold, 5.7-fold significant increases in *Hes5*, *Ngn2*, and *Dscam1* ($p < .05$) and a 3.4-fold reduction in *Calb1* ($p < .05$). **(D)** The GCL-ML subregion was microdissected from the HP of 2 month-old *Igf-1^{Ctrl}* and *Igf-1^{Δ/Δ}* mice and the mRNA isolated for qPCR analysis. Similar to that found in HPSCs the mRNA levels of *Hes5* and *Ngn2* in the GCL-ML were 2.2-fold and 1.5-fold (in \log_2 scale) and 4.7-fold and 2.8-fold greater in *Igf-1^{Δ/Δ}* mice compared to *Igf-1^{Ctrl}*. The level of *Igf-1* mRNA in the *Igf-1^{Δ/Δ}* GCL-ML dropped sharply (6.9-fold; $p < .001$). **(E)** aHPSC neurospheres from 6 month-old *Igf-1^{Ctrl}* and *Igf-1^{Δ/Δ}* mice were grown as described in the experimental design 2. **(F)** The images show representative immunostaining with anti-BrdU and anti-Ki67 antibodies and counterstained with Hoechst of aHPSCs. **(G)** The graphs represent the percentages of Ki67⁺ cells and of BrdU⁺Ki67⁻/BrdU⁺. The *Igf-1^{Δ/Δ}* cultures had higher percentage of Ki67⁺-cells whereas they showed a decrease in cell cycle exit. The results are the mean \pm SEM of 4–6 experiments performed in triplicate and of four independent cultures. **(H)** The images show representative immunostaining with anti-BrdU and anti-Ki67 antibodies and counterstained with Hoechst of vibratome sections from 2 month-old *Igf-1^{Ctrl}* and *Igf-1^{Δ/Δ}* mice. **(I)** The results (mean \pm SEM of 3–4 animals) show a 36% reduction (nonstatistically significant) in cells exiting the cell cycle in the *Igf-1^{Δ/Δ}* mice in vivo. Scale bar (F and H): F, 28.6 μ m; H, 29.1 μ m. Abbreviations: DIV, days in vitro; EGF, epidermal growth factor; FGF-2, fibroblast growth factor-2; GCL, granule cell layer; Igf-I, insulin-like growth factor-I; ML, molecular layer; SGZ, subgranular zone.

Dscaml1, an early marker of neuronal differentiation [48] and reducing that of *Calb1*, a late marker of neuronal differentiation [71]. Moreover, in the absence of IGF-I, cell cycle exit is partially inhibited in HPSCs.

DISCUSSION

Although there is evidence that IGF-I promotes neuronal formation and maintenance in the postnatal/adult HP [24, 25], the role of locally-produced IGF-I remains largely unknown and the stages and mechanisms by which IGF-I affects hippocampal neurogenesis have not been fully defined. Our results suggest that NSCs as well as PV neurons and possibly granule neurons, among other cells, may be the neural source of local IGF-I in the DG.

Here, we show that neuronal progenitors accumulate in the DG in the absence of IGF-I, which is also associated with the disorganization of the GCL and reduced dendrite growth of granule neurons. Thus, our stage-specific analysis of hippocampal neurogenesis in two mouse *Igf-1* lines (global and nervous system-specific) indicates that brain IGF-I regulates the number and location of dividing progenitors, and the correct positioning and differentiation of newly formed granule neurons in the GCL (Supporting Information Fig. S6B). Our findings suggest that the effects of IGF-I deficiency might be dependent on the upregulation of *Hes5* and *Ngn2* and the maintenance of cells in cycle, facts that could impair the transition from NSCs and progenitors to mature granule neurons.

The Effect of *Igf-1* Deletion on Hippocampal Neural Stem and Progenitor Cells

It was previously proposed that poorer survival rather than decreased proliferation provokes the reduction in the size of the HP of global *Igf-1*^{-/-} mice [24]. Here we found more cycling cells and Tbr2⁺-neuronal progenitors in the absence of IGF-I, which are distributed aberrantly in the outer areas of the GCL, and even in the ML. The larger size of the clonal neurospheres from *Igf-1*^{-/-} mice is compatible with an increase in the proliferation of progenitor cells corroborating the in vivo data. Notably, in the *Igf-1*^{Δ/Δ} mice, which in contrast to the global *Igf-1*^{-/-} mice (Baker et al. 1993; Beck et al. 1995; Cheng et al. 2001; Pichel et al. 2003) have normal body and brain weight, we also found an increase in the number and displacement of progenitors in the oGCL, together with a significant reduction of the GCL volume, although the size of the DG and the HP were not significantly diminished. Thus, the data obtained in the *Igf-1*^{Δ/Δ} mice support a specific role for brain IGF-I in regulating the number and position of neuronal progenitors, rather than this being a secondary effect due to the reduction of somatic or brain growth.

The increase in the number of cycling cells detected in the *Igf-1* KO mouse seems not to agree with previous data from studies into the action of exogenous IGF-I. Indeed, IGF-I stimulates the proliferation of embryonic NSCs [55, 72] and the overexpression or peripheral administration of IGF-I enhances the number of proliferative cells in the postnatal/adult HP [18, 22, 73]. By contrast and in line with our results, more proliferative cells in the postnatal SGZ of global *Igf-1* KO mice were previously reported [24]. Our novel findings showing greater *Hes5* and *Ngn2* expression and lower *Calb1*

expression in HPSCs and in the GCL-ML of *Igf-1*^{Δ/Δ} mice may suggest that the absence of brain IGF-I produces a deregulation of IGF-I/IGF-IR mediated intracellular signaling that may ultimately alter gene transcription. This would lead to enhanced proliferation and/or the maintenance of cells in cycle and therefore accumulation of dividing progenitor cells. In support of this idea, a greater number of dividing progenitors was found in the *Igf-1* knockout both in vitro and in vivo and cell cycle exit was partially reduced in HPSCs induced to differentiate in culture. Furthermore, downregulation of *Hes5* has been reported to be necessary for neuronal generation from HPSCs in the adult mouse [68, 74] and *Ngn2* overexpression favors the amplification of granule neuron progenitors [69]. Accordingly, we suggest that high levels of *Hes5* and *Ngn2* in *Igf-1*^{Δ/Δ} cells would favor the maintenance of cells as NSC and progenitors inhibiting the progression to terminal neuronal differentiation. However, this idea would need additional support as the increases in *Hes5* and *Ngn2* levels in HPSCs were significant but they did not reach statistical significance when the experiment was performed in the GCL-ML of *Igf-1*^{Δ/Δ} mouse.

It could also be possible that the above mentioned alterations favor the ectopic position of progenitor cells in the different subdivisions of the GCL. Furthermore, the disrupted RGC morphology may also impair the proper migration and positioning of neuronal progenitors and granule neurons (see next). Concurring with these ideas, altered IGF-I/IGF-IR intracellular pathways cause cell accumulation in the adult SVZ of *Igf-1*^{-/-} mice [12, 37], over-activation of the AKT signaling pathway alters neuronal positioning in the adult DG [75] and the interaction between RGCs and neuronal progenitors is necessary for DG formation [76].

The Effect of IGF-I on Neuronal Differentiation, Migration and Positioning in the DG

In the *Igf-1*^{-/-} mice, the accumulation of progenitor cells did not imply an increase in newly formed mature CB⁺-neurons but rather, we detected a fewer such cells and more immature DCX⁺- and CR⁺-granule cells in our retroviral injection experiments. It has been reported that only a subpopulation of progenitor cells generate mature neurons that functionally integrate into the DG, whereas the majority undergo apoptosis and are removed by phagocytosis [77]. In fact, loss of progenitors and/or reduced generation could explain the lower numbers of Pax6⁺- and Tbr2⁺-cells both in *Igf-1*^{+/+} and *Igf-1*^{-/-} mice at P49-54 compared to those at P21-23. A lack of *Igf-1* was previously reported to cause cell death and reduced neuronal survival in the DG [24, 26, 67] and a nestin-dependent conditional *Igf-IR* KO produces gross defects in the DG [17]. However, we did not observe an increase in apoptosis in histological sections or in cultured HPSCs, suggesting that the reduction in newly formed CB⁺-cells in the *Igf-1*^{-/-} mice was probably not due to the activation of cell death but rather to inhibited neuronal differentiation and maturation, as above mentioned.

In addition to affecting molecular differentiation, the lack of IGF-I prevents the correct morphological polarization and differentiation of granule neurons. In fact, the labeling of dividing cells and their neuronal progeny with retroviral vectors confirms the specific impact of *Igf-1* deletion on the morphology of neurons generated during the postnatal/adult

period. Moreover, our results indicate that local IGF-I promotes, in a paracrine and/or autocrine manner, the morphological differentiation of immature granule neurons as shown by the reduced length, and altered radial orientation of DCX⁺-neurites in the *Igf-1*^{Δ/Δ}.

The lack of *Igf-1* also produces a significant increase in the number of ectopic Prox1⁺- neurons that lie outside the GCL, probably due to the deregulation of IGF-I/IGF-IR mediated intracellular signaling and the disrupted morphology of RGC processes, as mentioned above to explain the aberrant position of neuronal progenitors. Supporting these ideas, the reduced complexity of RGC morphology in the OB of embryonic *Igf-1*^{-/-} mice concurs with deficits of mitral neuron migration [12, 55]. Although the number of Tbr2⁺- neuronal progenitors was significantly higher in P49-54 *Igf-1*^{-/-} mice, we did not find an aberrant distribution of these cells compared with that in P21-23 mice. This may reflect that the ectopic neuronal progenitors could have differentiated to Prox1⁺-neurons, which are displaced at P49-54.

It could not be excluded that the impact of *Igf-1* deletion in postnatal/adult hippocampal neurogenesis could be secondary to alterations that occur during embryonic development. However, when we stained sections from E18.5 *Igf-1*^{-/-} embryos with an anti-Prox1 antibody we found that the *Igf-1*^{-/-} mice had a slight delay in the formation of the ventral and dorsal blades of the DG (unpublished observations). By contrast, in the postnatal/adult DG significant numbers of granule neurons were found displaced. Our finding of the aberrant distribution of both neuronal progenitors and granule neurons in the *Igf-1*^{Δ/Δ} mice strongly suggests that local IGF-I influences migration and the correct final neuronal position in the postnatal/adult HP.

Concluding Remarks on the Role of Circulating and Brain IGF-I on Hippocampal Neurogenesis

The liver is the main source of IGF-I in the adult and it can cross the blood brain barrier to affect hippocampal neurogenesis particularly after physical exercise [11, 21, 78]. However, exercise can elicit both IGF-I dependent and independent effects on cycling cells, neuronal progenitors and postmitotic immature neurons [79]. Alternatively, other studies suggested the implication of locally-produced IGF-I in the modulation of adult hippocampal neurogenesis in vivo but this concept was not demonstrated [14, 24, 32–34, 67]. Here we report deficits in several steps of hippocampal neurogenesis in a nervous system specific KO mouse in which the level of serum IGF-I is indistinguishable from that in control mice whereas neural cells lack *Igf-1* mRNA almost completely. Since HPSCs and neurons express *Igf-1* mRNA, IGF-I and IGF-IR, paracrine and autocrine models could be claimed to explain the actions of IGF-I.

We cannot rule out that the accumulation of cycling cells observed in the global *Igf-1*^{-/-} mice may be compensated by circulating IGF-I in the *Igf-1*^{Δ/Δ} mice. In fact, the increase in total number cycling cells is not statistically significant in the conditional mice. However, the GCL of the conditional mice contains significantly more ectopic cycling cells than that of *Igf-1*^{ctrl} mice. In addition, our findings show that the number of neuronal progenitors, the generation of granule neurons as well as the migration/positioning and differentiation of these neurons are dependent on local IGF-I. Accordingly, IGF-I actions are not only cell-dependent but may also be modulated by the source of this growth factor.

In conclusion, we present novel findings showing that brain IGF-I is a fundamental component of the molecular network that instructs the sequential steps of the transition from NSCs and progenitors to mature granule neurons in the postnatal/adult HP (Supporting Information Fig. S6B).

ACKNOWLEDGMENTS

We wish to thank Dr. A. Lepier (Institute of Physiological Genomics, Muenchen) for sharing with us the 1F8 cells and protocols, Drs. D. LeRoith and S. Yakar (Mount Sinai School of Medicine, New York) for providing us with the *Igf-1* loxP mice, Drs. G. Provenzano and Y. Bozzi (University of Trento, Italy) for input on *Igf-1* in situ hybridization, and M.J. Román (Institute Cajal, Madrid) for her technical support. This work was funded by grants from the Spanish Ministerio de Ciencia e Innovación and Ministerio de Economía y Competitividad (MICINN and MINECO; BFU2007-61230, BFU2010-1963 and SAF2013-4759R, the Instituto de Salud Carlos III (ISCIII; CIBERNED CB06/05/0065), and the Comunidad de Madrid (S2011/BMD-2336) to C.V.-A.; and BFU2014-57494-R to A.V.M. V.N.-E was supported by a FPI Fellowship from the MICINN and MINECO.

AUTHOR CONTRIBUTIONS

V.N.-E.: Design, collection and assembly of data, data analysis and interpretation, manuscript writing. C.O.O.-M.: collection and assembly of data, data analysis and interpretation. L.L.: collection and assembly of data, data analysis and interpretation. J.P.: provision of study material. A.V.M.: collection and assembly of data, data analysis and interpretation, financial support. C.V.-A.: conception and design, data analysis and interpretation, financial support, manuscript writing and final approval of manuscript.

DISCLOSURE OF POTENTIAL CONFLICTS OF INTEREST

The authors declare that they have no conflicts of interest.

REFERENCES

- Eriksson PS, Perfilieva E, Björk-Eriksson T et al. Neurogenesis in the adult human hippocampus. *Nat Med* 1998;4:1313–1317.
- Gage FH, Temple S. Neural stem cells: Generating and regenerating the brain. *Neuron* 2013;80:588–601.
- Spalding KL, Bergmann O, Alkass K et al. Dynamics of hippocampal neurogenesis in adult humans. *Cell* 2013;153:1219–1227.
- Bonaguidi MA, Wheeler MA, Shapiro JS et al., In vivo clonal analysis reveals self-renewing and multipotent adult neural stem cell characteristics. *Cell* 2011;145:1142–1155.
- Encinas JM, Michurina TV, Peunova N et al., Division-coupled astrocytic differentiation and age-related depletion of neural stem cells in the adult hippocampus. *Cell Stem Cell* 2011;8:566–579.
- Hodge RD, Kahoud RJ, Hevner RF. Transcriptional control of glutamatergic differentiation during adult neurogenesis. *Cell Mol Life Sci* 2012;69:2125.
- Zhao C, Teng EM, Summers RG Jr et al. Distinct morphological stages of dentate granule neuron maturation in the adult mouse hippocampus. *J Neurosci* 2006;26:3–11.
- Faigle R, Song H. Signaling mechanisms regulating adult neural stem cells and neuro-

genesis. *Biochim Biophys Acta* 2013;1830:2435–2448.

- 9 Mu Y, Lee SW, Gage FH. Signaling in adult neurogenesis. *Curr Opin Neurobiol* 2010;20:416–423.
- 10 Agis-Balboa RC, Fischer A. Generating new neurons to circumvent your fears: The role of IGF signaling. *Cell Mol Life Sci* 2014; 71:21–42.
- 11 Fernandez AM, Torres-Aleman I. The many faces of insulin-like peptide signalling in the brain. *Nat Rev Neurosci* 2012;13:225–239.
- 12 Hurtado-Chong A, Yusta-Boyo MJ, Vergaño-Vera E et al., IGF-I promotes neuronal migration and positioning in the olfactory bulb and the exit of neuroblasts from the subventricular zone. *Eur J Neurosci* 2009;30: 742–755.
- 13 Vicario-Abejón C, Fernández-Moreno C, Pichel JG et al. Mice lacking IGF-I and LIF have motoneuron deficits in brain stem nuclei. *Neuroreport* 2004;15:2769–2772.
- 14 Bartke A, Sun LY, Longo V. Somatotropic signaling: trade-offs between growth, reproductive development, and longevity. *Physiol Rev* 2013;93:571–598.
- 15 Vogel T. Insulin/IGF-signalling in embryonic and adult neural proliferation and differentiation in the mammalian central nervous system. In: Sabine W-G, ed. *Trends in Cell Signaling Pathways in Neuronal Fate Decision*, 2013. InTech, DOI: 10.5772/54946. Available from: <http://www.intechopen.com/books/trends-in-cell-signaling-pathways-in-neuronal-fate-decision/insulin-igf-signalling-in-embryonic-and-adult-neural-proliferation-and-differentiation-in-the-mammal>
- 16 Nieto-Estévez V, Defferali C, Vicario-Abejón C. IGF-I: A key growth factor that regulates neurogenesis and synaptogenesis from embryonic to adult stages of the brain. *Front Neurosci* 2016;10:52.
- 17 Liu W, Ye P, O'Kusky JR et al. Type 1 insulin-like growth factor receptor signaling is essential for the development of the hippocampal formation and dentate gyrus. *J Neurosci Res* 2009;87:2821–2832.
- 18 Aberg MA, Aberg ND, Hedbäck H et al. Peripheral infusion of IGF-I selectively induces neurogenesis in the adult rat hippocampus. *J Neurosci* 2000;20:2896–2903.
- 19 Aberg MA, Aberg ND, Palmer TD et al. IGF-I has a direct proliferative effect in adult hippocampal progenitor cells. *Mol Cell Neurosci* 2003;24:23–40.
- 20 Trejo JL, Carro E, Torres-Aleman I. Circulating insulin-like growth factor I mediates exercise-induced increases in the number of new neurons in the adult hippocampus. *J Neurosci* 2001;21:1628–1634.
- 21 Trejo JL, Llorens-Martín MV, Torres-Aleman I. The effects of exercise on spatial learning and anxiety-like behavior are mediated by an IGF-I-dependent mechanism related to hippocampal neurogenesis. *Mol Cell Neurosci* 2008;37:402–411.
- 22 Yuan H, Chen R, Wu L et al. The regulatory mechanism of neurogenesis by IGF-1 in adult mice. *Mol Neurobiol* 2015;51:512.
- 23 O'Kusky JR, Ye P, D'Ercole AJ. Insulin-like growth factor-I promotes neurogenesis and synaptogenesis in the hippocampal dentate gyrus during postnatal development. *J Neurosci* 2000;20:8435–8442.
- 24 Cheng CM, Cohen M, Tseng V et al. Endogenous IGF1 enhances cell survival in the postnatal dentate gyrus. *J Neurosci Res* 2001;64:341–347.
- 25 Beck KD, Powell-Braxton L, Widmer HR et al. Igf1 gene disruption results in reduced brain size, CNS hypomyelination, and loss of hippocampal granule and striatal parvalbumin-containing neurons. *Neuron* 1995;14:717–730.
- 26 Liu W, D'Ercole JA, Ye P. Blunting type 1 insulin-like growth factor receptor expression exacerbates neuronal apoptosis following hypoxic/ischemic injury. *BMC Neurosci* 2011; 12:64.
- 27 Li Y, Komuro Y, Fahrion JK et al. Light stimuli control neuronal migration by altering of insulin-like growth factor 1 (IGF-1) signaling. *Proc Natl Acad Sci U S A* 2012;109:2630–2635.
- 28 Maucksch C, McGregor AL, Yang M et al. IGF-I redirects doublecortin-positive cell migration in the normal adult rat brain. *Neuroscience* 2013;241:106–115.
- 29 Onuma TA, Ding Y, Abraham E et al. Regulation of temporal and spatial organization of newborn GnRH neurons by IGF signaling in zebrafish. *J Neurosci* 2011;31:11814–11824.
- 30 Xiang Y, Ding N, Xing Z et al. Insulin-like growth factor-1 regulates neurite outgrowth and neuronal migration from organotypic cultured dorsal root ganglion. *Int J Neurosci* 2011;121:101–106.
- 31 Bartlett WP, Li XS, Williams M et al. Localization of insulin-like growth factor-1 mRNA in murine central nervous system during postnatal development. *Dev Biol* 1991; 147:239–250.
- 32 Carlson SW, Madathil SK, Sama DM et al. Conditional overexpression of insulin-like growth factor-1 enhances hippocampal neurogenesis and restores immature neuron dendritic processes after traumatic brain injury. *J Neuropathol Exp Neurol* 2014;73: 734–746.
- 33 Shetty AK, Hattiangady B, Shetty GA. Stem/progenitor cell proliferation factors FGF-2, IGF-1, and EGF exhibit early decline during the course of aging in the hippocampus: Role of astrocytes. *Glia* 2005;51:173–186.
- 34 Zhang J, Moats-Staats BM, Ye P et al. Expression of insulin-like growth factor system genes during the early postnatal neurogenesis in the mouse hippocampus. *J Neurosci Res* 2007;85:1618–1627.
- 35 Liu JP, Baker J, Perkins AS et al. Mice carrying null mutations of the genes encoding insulin-like growth factor I (Igf-1) and type 1 IGF receptor (Igf1r). *Cell* 1993;75:59–72.
- 36 Pichel JG, Fernández-Moreno C, Vicario-Abejón C et al. Developmental cooperation of leukemia inhibitory factor and insulin-like growth factor I in mice is tissue-specific and essential for lung maturation involving the transcription factors Sp3 and TTF-1. *Mech Dev* 2003;120:349–361.
- 37 Otaegi G, Yusta-Boyo MJ, Vergano E et al. Modulation of the PI 3-kinase-Akt signaling pathway by IGF-I and PTEN regulates the differentiation of neural stem/precursor cells. *J Cell Sci* 2006;119(Pt 13): 2739–2748.
- 38 Liu JL, Grinberg A, Westphal H, Sauer B, Accili D, Karas M, LeRoith, D. Insulin-like growth factor-I affects perinatal lethality and postnatal development in a gene dosage-dependent manner: manipulation using the Cre/loxP system in transgenic mice. *Mol Endocrinol* 1998;12:1452–1462.
- 39 Josephson R, Müller T, Pickel J et al. POU transcription factors control expression of CNS stem cell-specific genes. *Development* 1998;125:3087–3100.
- 40 Panchision DM, Pickel JM, Studer L et al. Sequential actions of BMP receptors control neural precursor cell production and fate. *Genes Dev* 2001;15:2094–2110.
- 41 Tronche F, Kellendonk C, Kretz O et al. Disruption of the glucocorticoid receptor gene in the nervous system results in reduced anxiety. *Nat Genet* 1999;23:99–103.
- 42 Srinivas S, Watanabe T, Lin C-S et al. Cre reporter strains produced by targeted insertion of EYFP and ECFP into the ROSA26 locus. *BMC Dev Biol* 2001;1:4.
- 43 Heinrich C, Gascón S, Masserdotti G et al. Generation of subtype-specific neurons from postnatal astroglia of the mouse cerebral cortex. *Nat Protoc* 2011;6:214–228.
- 44 Mendez-Gomez HR, Vergaño-Vera E, Abad JL et al. The T-box brain 1 (Tbr1) transcription factor inhibits astrocyte formation in the olfactory bulb and regulates neural stem cell fate. *Mol Cell Neurosci* 2011;46:108–121.
- 45 Galeeva A, Treuter E, Tomarev SI et al. A prospero-related homeobox gene Prox-1 is expressed during postnatal brain development as well as in the adult rodent brain. *Neuroscience* 2007;146:604–616.
- 46 Iwano T, Masuda A, Kiyonari H et al. Prox1 postmitotically defines dentate gyrus cells by specifying granule cell identity over CA3 pyramidal cell fate in the hippocampus. *Development* 2012;139:3051–3062.
- 47 Vergaño-Vera E, Méndez-Gómez HR, Hurtado-Chong A et al. Fibroblast growth factor-2 increases the expression of neurogenic genes and promotes the migration and differentiation of neurons derived from transplanted neural stem/progenitor cells. *Neuroscience* 2009;162:39–54.
- 48 Nieto-Estévez V, Pignatelli J, Araúzo-Bravo MJ et al. A global transcriptome analysis reveals molecular hallmarks of neural stem cell death, survival, and differentiation in response to partial FGF-2 and EGF deprivation. *PLoS One* 2013;8:e53594.
- 49 Schmittgen TD, Livak KJ. Analyzing real-time PCR data by the comparative C(T) method. *Nat Protoc* 2008;3:1101–1108.
- 50 Curto GG, Nieto-Estévez V, Hurtado-Chong A et al. Pax6 is essential for the maintenance and multi-lineage differentiation of neural stem cells, and for neuronal incorporation into the adult olfactory bulb. *Stem Cells Dev* 2014;23:2813–2830.
- 51 Russo VC, Gluckman PD, Feldman EL et al. The insulin-like growth factor system and its pleiotropic functions in brain. *Endocr Rev* 2005;26:916–943.
- 52 Bach MA, Shen-Orr Z, Lowe WL Jr et al. Insulin-like growth factor I mRNA levels are developmentally regulated in specific regions

of the rat brain. *Brain Res Mol Brain Res* 1991;10:43–48.

- 53** Bondy CA, Lee WH. Patterns of insulin-like growth factor and IGF receptor gene expression in the brain. *Functional implications.* *Ann N Y Acad Sci* 1993;692:33–43.
- 54** Rotwein P, Burgess SK, Milbrandt JD et al. Differential expression of insulin-like growth factor genes in rat central nervous system. *Proc Natl Acad Sci U S A* 1988;85:265–269.
- 55** Vicario-Abejón C, Yusta-Boyo MJ, Fernández-Moreno C et al. Locally born olfactory bulb stem cells proliferate in response to insulin-related factors and require endogenous insulin-like growth factor-I for differentiation into neurons and glia. *J Neurosci* 2003;23:895–906.
- 56** Lee CH, Ahn JH, Park JH et al. Decreased insulin-like growth factor-I and its receptor expression in the hippocampus and somatosensory cortex of the aged mouse. *Neurochem Res* 2014;39:770–776.
- 57** Garcia-Segura LM, Pérez J, Pons S et al. Localization of insulin-like growth factor I (IGF-I)-like immunoreactivity in the developing and adult rat brain. *Brain Res* 1991;560:167–174.
- 58** Riquelme R, Cediel R, Contreras J et al. A comparative study of age-related hearing loss in wild type and insulin-like growth factor I deficient mice. *Front Neuroanat* 2010;4:27.
- 59** Baker J, Liu JP, Robertson EJ et al. Role of insulin-like growth factors in embryonic and postnatal growth. *Cell* 1993;75:73–82.
- 60** McKay R. Stem cells in the central nervous system. *Science* 1997;276:66–71.
- 61** Suh H, Consiglio A, Ray J et al. In vivo fate analysis reveals the multipotent and self-renewal capacities of Sox2 + neural stem cells in the adult hippocampus. *Cell Stem Cell* 2007;1:515–528.
- 62** Mendez-Gomez HR, Vicario-Abejón C. The homeobox gene *Gsx2* regulates the self-renewal and differentiation of neural stem cells and the cell fate of postnatal progenitors. *PLoS One* 2012;7:e29799.
- 63** von Bohlen und Halbach O. Immunohistological markers for proliferative events, gliogenesis, and neurogenesis within the adult hippocampus. *Cell Tissue Res* 2011;345:1–19.
- 64** Hsieh J. Orchestrating transcriptional control of adult neurogenesis. *Genes Dev* 2012;26:1010–1021.
- 65** Hodge RD, Kowalczyk TD, Wolf SA et al. Intermediate progenitors in adult hippocampal neurogenesis: *Tbr2* expression and coordinate regulation of neuronal output. *J Neurosci* 2008;28:3707–3717.
- 66** Gleeson JG, Lin PT, Flanagan LA et al. Doublecortin is a microtubule-associated protein and is expressed widely by migrating neurons. *Neuron* 1999;23:257–271.
- 67** Lichtenwalner RJ, Forbes ME, Sonntag WE et al. Adult-onset deficiency in growth hormone and insulin-like growth factor-I decreases survival of dentate granule neurons: insights into the regulation of adult hippocampal neurogenesis. *J Neurosci Res* 2006;83:199–210.
- 68** Lugert S, Basak O, Knuckles P et al. Quiescent and active hippocampal neural stem cells with distinct morphologies respond selectively to physiological and pathological stimuli and aging. *Cell Stem Cell* 2010;6:445–456.
- 69** Roybon L, Hjalt T, Stott S et al. *Neurogenin2* directs granule neuroblast production and amplification while *NeuroD1* specifies neuronal fate during hippocampal neurogenesis. *PLoS One* 2009;4:e4779.
- 70** Imayoshi I, Kageyama R. bHLH factors in self-renewal, multipotency, and fate choice of neural progenitor cells. *Neuron* 2014;82:9–23.
- 71** Vicario-Abejón C, Johe KK, Hazel TG et al. Functions of basic fibroblast growth factor and neurotrophins in the differentiation of hippocampal neurons. *Neuron* 1995;15:105–114.
- 72** Mairret-Coello G, Tury A, DiCicco-Bloom E. Insulin-like growth factor-1 promotes G(1)/S cell cycle progression through bidirectional regulation of cyclins and cyclin-dependent kinase inhibitors via the phosphatidylinositol 3-kinase/Akt pathway in developing rat cerebral cortex. *J Neurosci* 2009;29:775–788.
- 73** Popken GJ, Hodge RD, Ye P et al. In vivo effects of insulin-like growth factor-I (IGF-I) on prenatal and early postnatal development of the central nervous system. *Eur J Neurosci* 2004;19:2056–2068.
- 74** Matsuda S, Kuwako K, Okano HJ et al. *Sox21* promotes hippocampal adult neurogenesis via the transcriptional repression of the *Hes5* gene. *J Neurosci* 2012;32:12543–12557.
- 75** Kim JY, Duan X, Liu CY et al. *DISC1* regulates new neuron development in the adult brain via modulation of AKT-mTOR signaling through KIAA1212. *Neuron* 2009;63:761–773.
- 76** Brunne B, Franco S, Bouché E et al. Role of the postnatal radial glial scaffold for the development of the dentate gyrus as revealed by Reelin signaling mutant mice. *Glia* 2013;61:1347–1363.
- 77** Sierra A, Encinas JM, Deudero JJ et al. Microglia shape adult hippocampal neurogenesis through apoptosis-coupled phagocytosis. *Cell Stem Cell* 2010;7:483–495.
- 78** Nishijima T, Piriz J, Duflot S et al. Neuronal activity drives localized blood-brain-barrier transport of serum insulin-like growth factor-I into the CNS. *Neuron* 2010;67:834–846.
- 79** Llorens-Martín M, Torres-Alemán I, Trejo JL. Exercise modulates insulin-like growth factor 1-dependent and -independent effects on adult hippocampal neurogenesis and behaviour. *Mol Cell Neurosci* 2010;44:109–117.



See www.StemCells.com for supporting information available online.